Front. Archit. Civ. Eng. China 2010, 4(1): 1–39
DOI 10.1007/s11709-010-0013-6

RESEARCH ARTICLE

Eduardo E. ALONSO, Rafaela CARDOSO

Behavior of materials for earth and rockfill dams: Perspective from unsaturated soil mechanics

Abstract The basis of the design of earth and rockfill dams is focused on ensuring the stability of the structure under a set of conditions expected to occur during its life. Combined mechanical and hydraulic conditions must be considered since pore pressures develop during construction, after impoundment and in drawdown. Other instability phenomena caused by transient flow and internal erosion must be considered. The prediction of the hydro-mechanical behavior of traditional and non-traditional materials used in the construction of dams is therefore fundamental. The materials used for dam's construction cover a wide range from clayey materials to rockfill. In a broad sense they are compacted materials and therefore unsaturated materials. A summary of the current level of knowledge on the behavior of traditional materials used in the construction of dams is presented in the paper. Regular compacted materials (with a significant clay fraction), rockfill and compacted soft rocks are studied with more detail. The latter are non-traditional materials. They are analysed because their use, as well as the use of mixtures of soil and rock, is becoming more necessary for sustainability reasons.

Keywords dams, unsaturated soil mechanics, suction, rockfill, clayey soil, mixture

1 Introduction

The basis of the design of earth and rockfill dams is focused on ensuring the stability of the structure under a set of conditions expected to occur during its life. The stability of the upstream and downstream slopes must be guaranteed at the end of the construction but also during reservoir impoundment and the operational phase, including drawdown and long-term steady state conditions as a limiting case. A fundamental aspect of the analysis is the generation of pore pressures during the construction and during the first filling, reservoir impounding and cases of rapid drawdown. Other aspects are also of concern, such as the deformation of the structure during the construction and operational stages, and also incidents caused by hydraulic fracture, internal erosion, long term effects and other combined cases.

Failures associated with hydraulic fracture and internal erosion is largely reported in the literature. Two recent cases of failure caused by collapse and internal erosion are presented in the first part of the paper. The hydro-mechanical behavior of the materials used in the construction of the earth structures are used to explain their failure.

An additional source of complexity is the fact that different types of materials are used. For traditional dams, impervious clayey materials are used for the core, rockfill materials (any type of rock) are used for shells and granular materials are used for filters. However, for sustainability constraints and environmental reasons, the use of marginal materials, i.e., materials that traditionally would not be used in the construction of dams, is becoming frequent. Such is the case of soft rocks or evolving rocks and soil or rock formations with some proportion of evaporites.

Figure 1 is a photograph of Lechago Dam in Teruel, Spain. A very traditional design was adopted. Three distinct zones can be distinguished: the core, built with regular compacted soils (low to medium plasticity sandy clays, clayey sands and clays), the shoulders built with indurated shale rockfill and the filter built with fine granular materials. Other solutions are also adopted in the design as a consequence of the available material for the construction. For example, rockfill materials can be used combined with solutions adopting impervious materials, as well as compacted soft rocks. Figure 2 shows the rockfill slopes of Caracoles Dam in San Juan, Argentina, a combined solution using rockfill, made of alluvial

Received July 17, 2009; accepted October 28, 2009

Eduardo E. ALONSO (✉)
Universidad Politécnica de Cataluña, Barcelona, Spain
E-mail: eduardo.alonso@upc.edu

Rafaela CARDOSO
Instituto Superior Técnico, Lisbon, Portugal

Fig. 1 Photograph of Lechago Dam showing the clay core, the filters and the rockfill shoulders

Fig. 2 Rockfill dam – Caracoles Dam

boulders, gravels and sands, and an upstream concrete diaphragm.

Compacted soft rocks are also used in the construction of dams and Albagés Dam, Lleida (Spain) is an example (Figure 3 shows an experimental embankment being built during the design of this dam). Compacted soft rocks (fragments of evolving rocks such as schist, marls and other clayey rocks) are different from rockfill (fragments of hard rock) because of the geological nature of the rocks used. After compaction and hydration, the large fragments of soft rock degrade and result in a material intermediate between soil and rock, relatively impervious, but more compressible and more sensitive to wetting and drying cycles than traditional rockfill.

Fig. 3 Construction of a trial embankment for Albagés Dam

Mixtures of rock and fine materials are other alternative materials. The characterization of their hydraulic and mechanical properties is usually complex because it depends on the nature of the materials, the proportions used and many other factors. Figure 4 is a photograph of the material used to build Villaveta Dam in Navarra, Spain (a natural mixture of gravels with clayey soil).

Each type of material has a unique behavior and its own particularities should be considered in dam design. Experience earned in the past decades is being used in design when traditional materials are adopted. Because it is no longer feasible to select "the best" emplacement or to import "good" materials, virtually any kind of soil or rock is expected to be used in the design of dams. Moreover, as new projects are being commissioned in Africa, South America and Asia, local soils and rocks outcropping in tropical and volcanic areas must be used. These soils are not understood as much as the "regular" sedimentary and alluvial formations found in temperate climates of the northern hemisphere. The use of non-traditional materials is an important challenge for a soil engineer. Concepts of unsaturated soil mechanics offer a sufficient degree of development to provide theories and models of compacted soil behavior, specialized testing and computational tools, which could improve the current state of the art on earth dam and rockfill engineering.

Fig. 4 Mixtures of gravels with fine soils (Villaveta Dam)

2 Two failures

Two cases are presented where collapse deformations were followed by internal erosion. The first case concerns an uncontrolled and dangerous leak and the second the rupture of a dam caused by localized collapse during impoundment.

2.1 Differential collapse of foundation during the first filling

The La Molina pond was built for water storage in the Catalonian Pyrenees. As shown in the plan view in Fig. 5, a 15 m high rockfill dam covered by an impervious membrane was built taking advantage of the topographic conditions. A pipe system (see Fig. 5) was included for drainage under the membrane. It was buried in a gravel and sand fill layer. No special attention was taken in the compaction of this fill layer, which was done probably dry of optimum.

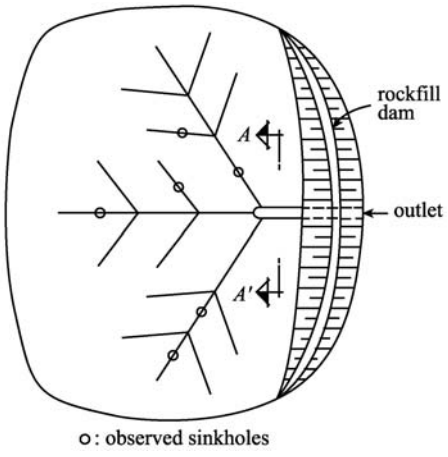

Fig. 5 Plan view of La Molina pond and drainage system

A few sinkholes were observed after full impoundment. Water whirlpools marked their position directly above drainage pipes (see sketch in Fig. 5). There were attempts to plug the holes by means of cement bags thrown from helicopters. The desperate procedure was partly successful but it was eventually decided to empty the pond.

Tunnel-shaped depressions were discovered at the whirlpool positions. The membrane was ruptured in those points. The granular base was excavated and the pipe drains were uncovered (see Fig. 6). They were found broken and filled, in relatively long distances, with a granular material. High speed water was capable of dragging the gravels inside the filter pipes.

Fig. 6 Drainage pipes filled with the material from the gravel and sand fill layer

A possible explanation for the failure is described as follows (see Fig. 7): Hydrostatic loading after impoundment caused probably some initial differential settlements of the gravel and sand fill, poorly compacted. However, it is believed that the progressive saturation of this granular layer, under the total stresses transmitted by the water level in the pond, led to a soil collapse, which was non-homogeneous. Then the differential collapse led to the breakage of the pipes at some points. Sand and gravel entering the pipes created local subsidence troughs, which eventually caused the breakage of the membrane under the water head of the pond. Once the membrane broke, the local erosion of the granular layer could enlarge the initial rupture. Water had a free escape at those points.

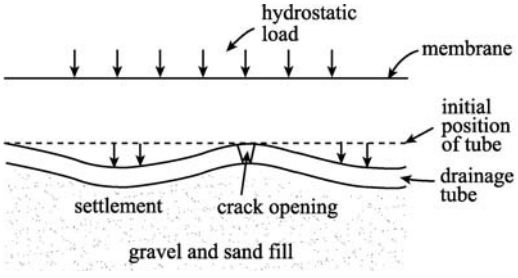

Fig. 7 Differential collapse of fill causing rupture of drainage pipes

This case was not developed further but it illustrates the need to ensure good compaction conditions of all the materials. They must be adequate to minimize the penalizing effects of their expected behavior in case of being fully saturated either in service conditions or by accident.

2.2 Fill collapse during impoundment

An artificial pond was created in an arid environment by building a homogeneous dam covered upstream by an impervious HDPE membrane. The construction took advantage of the ground topography so that the dam was necessary only in part of the pond perimeter, as shown in Fig. 8. The dam was built having a maximum height of 20 m at the location of the creek, but progressively decreased in height in the rest of the dyke perimeter. Figure 8 shows a sketch of the small watershed area drained by a small creek. Figure 9 shows the dam cross section at the position of the original creek draining the area later occupied by the pond.

Low plasticity sandy clays and high plasticity clays were compacted within short distances within the embankment. There are also indications that the achieved field densities were lower than the optimum Normal Proctor values. Wetting under load tests performed on some specimens

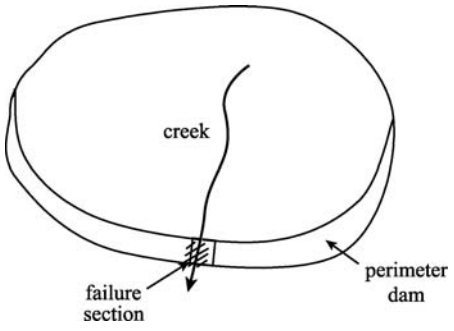

Fig. 8 Artificial pond and dam built over small creek

indicated a high collapse potential. In two tests performed, collapse deformations reached values of 3.8% (for a vertical load of 85 kPa) and 8.3% (for a vertical load of 245 kPa). These two vertical loads are well within the range of vertical stresses expected within the maximum cross section given in Fig. 9.

On first impoundment, when the water level reached 15 m over the foundation, a section of the dam, located directly above the position of the creek, failed, causing a violent flood. Figures 10 and 11 show the failed section. The development of the failure was not observed. When the photographs in Figs. 10 and 11 were taken, the reservoir was practically empty.

Field observations (see Fig. 12) indicated that the fill could have a significant collapse potential and, probably, a susceptibility to internal erosion. Troughs and sinkholes were observed in the downstream slope of the dam a few years after the collapse. The compacted soils (they are observed in the background of Fig. 12, where the almost vertical slope of the failed section remained stable a few years after the dam failure) were rather heterogeneous.

It is acceptable to assume that any rain water falling into the pond area during construction was eventually drained out through the creek bed. This situation could only change in the final stage of the works, when the HDPE membrane covered the pond and the upstream slopes of the dam. A strong indicator that water percolating in the creek was related with the collapse observed is the fact that, a few years after the failure, stumps at the creek grew green and gave rise to new trees in their ancient locations. This is an indication of the imperfect cleaning operations of the creek before the construction of the dam.

A possible explanation for the failure is described as follows:

Insufficient compaction of the fill, probably dry of optimum, builds a collapse potential into the fill. This collapse potential develops when a given point within the fill experiences an increase in confining stress over the initial yield stress induced by compaction. The collapse strains will develop if the water content increases.

The fill located immediately above the creek holds the most critical situation: here, the dam reaches the maximum height and the seeping waters through the creek bed could easily lead to a capillary rise affecting a certain thickness above the original ground level. Therefore, the fill volume having the highest collapse potential is viewed as an elongated mass of compacted soil lying directly above the creek. A collapse of this volume will tend to create voids and cracks, which could lead to a preferential path connecting the upstream and downstream slopes of the dam.

Additional field observations indicated that the polyethylene membrane penetrated into the upstream slope, adopting funnel-like shapes, forced by the water hydrostatic force. These symptoms are also interpreted as an indication of the collapse potential of the fill. Voids were also observed in the lateral nearly vertical cuts into the fill left by the failure.

It is believed that the membrane broke when forced by the water pressure into a collapsing soil, located upstream immediately above the creek position. Once the membrane was broken, the water under pressure found a preferential path of interconnected voids and cracks, which extended from upstream to downstream, above the creek location, creating a "tunnel" inside the fill, which increased in size and eventually collapsed, leaving a breach of approximately rectangular shape in cross section (see Fig. 10).

Simulation of the entire process is a major challenge, but the preceding explanation could be supported by some analysis even if it only covers some partial aspects. Consider in Fig. 13(a) a central vertical section through the dam longitudinal axis. A simplified geometry to analyze the collapse effects induced by creek wetting is shown in Fig. 13(b). The creek position becomes a point where wetting is simulated by imposing the condition of zero suction. The remaining fill maintains the expected suction after compaction and layer-by-layer construction. A simple two-dimensional model (in plane strain) was solved with the help of CODE_BRIGHT [1,2]. The model dimensions

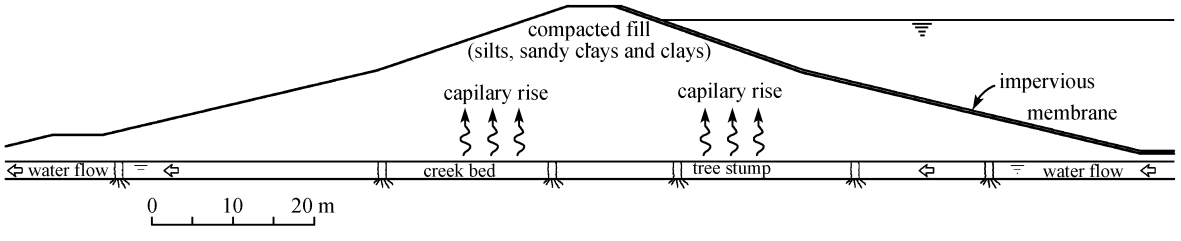

Fig. 9 Representative cross section of dam

Fig. 10 Downstream view of dam after failure

are 100 m (horizontal dimension) by 20 m (vertical dimension). It was "built" in 500 days, assuming an initial porosity $n = 0.5$ and initial suction $s = 3$ MPa.

A simulated collapse test under a vertical stress of 200 kPa is shown in Fig. 14. The model in this case predicts a collapse of 5.5% for a full wetting. Starting at an initial suction of 3 MPa, these collapse strains are believed to approximate actual "in situ" conditions. Boundaries were considered impervious during this phase. Then the suction in the lower centred point was brought to zero. Vertical stresses around this wetting point began to change at a rate controlled by the soil permeability.

Model parameters were approximated from some available laboratory data. In particular, collapse tests provided important information to approximate most of Barcelona basic model (BBM) parameters presented later in the text. The parameters selected are given in Table 1.

Results are shown in Fig. 15. Arching effects are clear in the figure. Points above the creek position experience a reduction in stress, compensated by an increase away from the wetting point. The final result of collapse and unloading phenomena is a decrease in porosity, indicating a trend towards the development of open voids (this is the case if the reduction in porosity concentrates on preferential planes, namely the planes between compaction layers).

The numerical results show, in a qualitative way, the mechanism proposed for the collapse. This dam failure highlights the risks associated with differential collapse inside an embankment structure. This differential collapse may be triggered by localized and progressive wetting

Fig. 11 Upstream view of dam after failure

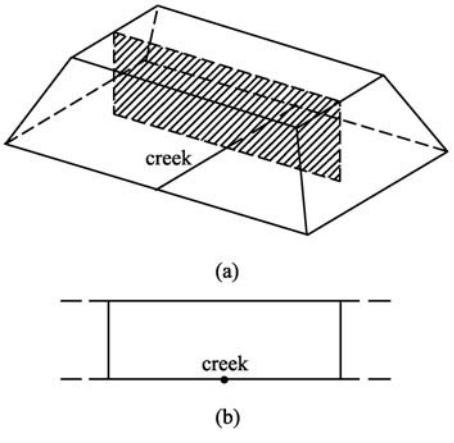

Fig. 13 Simulation of process. (a) Longitudinal central plane and position of creek; (b) two-dimensional representation

Fig. 12 Field indicators of the collapse potential of the fill

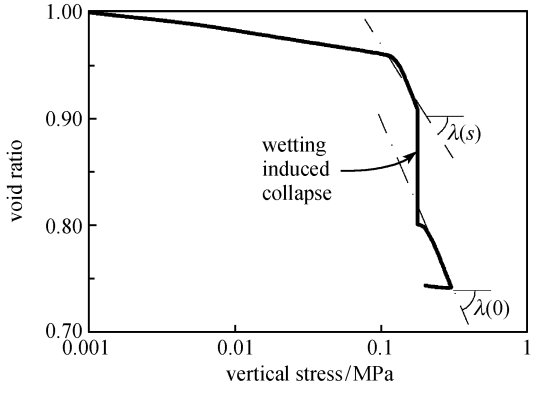

Fig. 14 Collapse test simulated with the adopted BBM model [3]

Table 1 Set of model parameters for fill [3]

mechanical parameters –Barcelona basic model (BBM)		
k	elastic compressibility	0.008
$\lambda(0)$	saturated virgin compressibility	0.1
r	parameter defining LC curve	0.5
β	parameter defining LC curve	12 MPa^{-1}
p_c	reference stress	0.02 MPa
v	Poisson's ratio	0.3
M	critical state slope	1
hydraulic parameters		
K	saturated intrinsic permeability (isotropic)	10–12 m^2
p_o	parameter of V. Genuchten model	0.24 MPa
λ	shape of V. Genuchten model	0.5
λ_r	power for relative permeability ($K_r = S_r\lambda_r$)	3

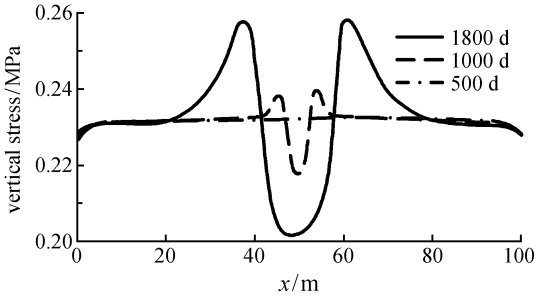

Fig. 15 Evolution of vertical stresses in plane located 2 m above base during wetting of central lower point (creek location)

processes (this is the case discussed here) or by other situations (differential stiffness, for instance). Of course, the original and fundamental risk is associated with the inherent high collapse potential of an insufficiently compacted soil, especially if compacted on the dry side. This conclusion is also valid for the first case described.

These two cases illustrate the insight that unsaturated soil mechanics may offer to understand the behavior of compacted dams. It also shows the capabilities of current computational models to analyze field situations. These two aspects: understanding and modeling are key issues discussed in this paper.

3 Unsaturated soil mechanics

It is usual in the technical and scientific literature to mention "unsaturated soils" as a well-defined area of knowledge which has an established theoretical background to interpret soil behavior. However, when dealing with saturated soils, the particular class of soils or a specific geotechnical issue is always described. A similar distinction must be done in unsaturated soils because general theories cover limited aspects of behavior. Recently, Alonso and co-workers [4] distinguished the following types of unsaturated materials: rockfill, sands and granular materials, regular compacted soils, compacted soft rocks and cemented materials. The classes are defined not only because they occupy well defined and separate positions in the scale of particle size or because they are expected to behave in a widely different manner from each other, but because their deformation mechanisms, associated with the state of the water in the pore space, are fundamentally different. Water influence on the mechanical behavior is described in Section 3.1, which describes some concepts used in unsaturated soil mechanics.

Among the materials traditionally used in the construction of earth and rockfill dams, the unsaturated soil types to be considered can be divided into regular compacted soils (with or without a significant clay fraction) and rockfill. They will be described with more detail in Section 3.2 because the experience earned in the last few decades allows the definition of constitutive models for each case in a quite satisfactory manner.

Advances are also being done for the characterization of non-traditional materials used in the construction of dams and earth embankments. Such is the case of compacted soft rocks and of mixtures of soil and rock. The prediction of deformations of structures built with these materials requires the definition of adequate unsaturated constitutive models. This is a current research topic.

Mixtures can integrate different or similar materials. When different, the behavior is expected to be intermediate between clayey soils and rockfill, depending on the proportions of the predominant grading sizes and the nature of the materials used. When the same material is mixed, the name mixture still can be used if very different grading sizes of the components are verified. Compacted soft rocks are an example of such mixture materials. The construction process (energy and hydration conditions) is particularly important in the definition of the proportions of the mixture which combine relatively large fragments and fine materials (passing sieve ASTM #200, $D < 0.075$ mm). Figure 16 shows the grading size curves before and after the compaction of Abadia marl fragments used in the construction of a motorway embankment in Arruda dos Vinhos (Portugal). The compaction process (heavy compaction and water content near the optimum value) results in an increase of the average percentage of the fine fraction from 43% to 78%.

In case of using evolving materials, the proportions of each component of the mixture may change along time due to degradation phenomena. Changes in global behavior are therefore expected. This case is analyzed in this section and also in Section 3.2.

Finally, the summary of the main features of behavior and hints on the appropriate constitutive modeling to be used in each case is given in Section 3.3. The main differences in terms of hydro-mechanical behavior of the unsaturated soil types analyzed are highlighted, justifying

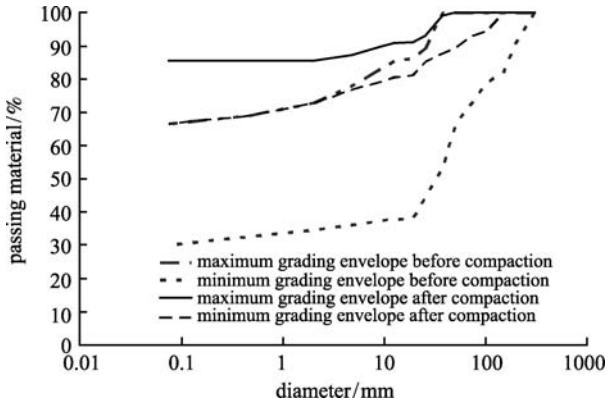

Fig. 16 Grading size distribution curves before and after the compaction of marl fragments [5]

the need of using different constitutive models adapted to each specific case.

3.1 Some concepts in unsaturated soil mechanics

3.1.1 Storage of water capacity: water retention curve

The soil water retention curve (WRC) is a measure of the storage water capacity of the soil when it is subjected to different values of suction. Storage water is expressed in terms of the gravimetric water content, w, the volumetric water content, θ, water ratio (volume of water over volume of solids) or degree of saturation, S_r. The features of WRC depend on soil properties such as type of soil, mineralogy, particle size distribution, soil structure (arrangement of particles or/and aggregates) and void ratio as well as on the direction of water content changes (wetting and drying) [6–9]. A detailed state of the art of the water retention characteristics of soils can be found in Refs. [10,11].

The effect of the structure and void ratio on the water storage capacity of a given soil has been highlighted in several experimental investigations [12–15]. As pointed out by several authors [11,14,16], two mechanisms generally govern the storage of water inside a soil. The first mechanism is mainly related to free water flow inside the macropores and the second one is related with the water adsorption at the intra-aggregate level, when it exists. This last mechanism seems to be independent of the macro-structure, whereas the amount of water stored in the macropores (per unit volume of soil) will be strongly affected by the changes in macro void ratio. As a consequence, swelling-collapse, shrinkage and loading paths, as well as contracting or dilating behavior as a result of shear strains, affects WRC [17]. Irreversible changes in degree of saturation or water content [12,18,19] during plastic volumetric strain due to isotropic loading at constant suction show also this hydro-mechanical coupling.

Figure 17 shows the loading paths of a sample of compacted kaolinitic-illitic clay subjected to oedometric loading [17] and the effect of different void ratio in WRC. Changes in volumetric strain (ε_v) are measured by changes in void ratio (e) and degree of saturation (S_r), for a given suction, and are illustrated by the water ratio (e_w) ($e_w = V_w/V_s$ where V_w is the volume of water and V_s is the volume of solid).

Experimental results on specimens of Barcelona silty clay [20] show irreversible collapse volumetric strain at constant net vertical stress taking place during wetting. Irreversible changes are also registered in water ratio and degree of saturation indicating the effect of the new arrangement of the solid particles on the hydraulic parameters. During subsequent loading at constant suction compressible volumetric deformation takes place. According to basic constitutive models for unsaturated soil, such as the models discussed in the introduction of this section (having a unique retention curve independent of void ratio), the reduction in void ratio at constant suction would imply a reduction in water content in order to maintain a constant degree of saturation (corresponding to the current suction). However, experimental results, although showing a reduction of the amount of water, indicate that the out flow water is lower than the amount predicted by a basic model. This results in an increment of degree of saturation. In addition, second loading-unloading cycle after a wetting induces irreversible changes in e, e_w and S_r and larger plastic deformation takes place involving a considerable increment in degree of saturation whereas water content remains essentially constant. These results, and others [21–23], indicate that at a given suction, the lower the void ratio, the higher degree of saturation held in equilibrium.

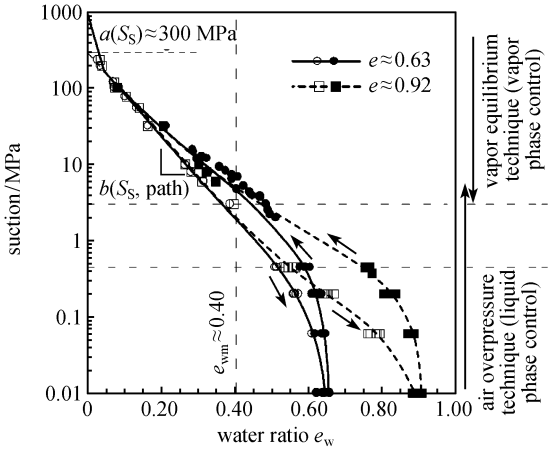

Fig. 17 Main wetting and drying retention curves at constant volume of compacted kaolinitic-illitic clay [17]

Water retention curves are also modified by changes in void ratio due to shearing strains. This was illustrated in Ref. [24]. The results show a significant increase in degree of saturation during shearing at constant suction and

constant mean net stress. This increment was attributed to the substantial decreases in void ratio that occurred.

The hydraulic hysteresis in the inflow or outflow of water into the soil voids is also observed in Fig. 17. It has been reported by many authors [6,14,25]. The physical explanation of the phenomena of hydraulic hysteresis results from microstructural considerations of the irreversible movement of the air water interface during the process of wetting and drying [13,26].

An accurate prediction of the mechanical behavior of the soil requires a precise description of the hydraulic behavior and in particular of the irreversible features of WRC. Experimental evidences and theoretical considerations have been published supporting this idea [27].

3.1.2 Stress states in unsaturated soils

The presence of water affects also the stresses to be considered in constitutive modeling. For example, the menisci of water that appear in the contact between solid particles presented in Fig. 18 generate an additional compressive force at this contact. When two planar surfaces are in contact and its interstitial water is in equilibrium with a given suction, the net attraction force between particles may reach high values. Figure 18 shows the dimensionless force between two spheres limited by a common planer surface [28], defined by the geometrical parameters β and ε shown in the figure.

If compared with the classical Fisher equation for the force induced by a thoroidal meniscus between two spheres, the presence of a planar surface with a given rugosity leads to a large increase of the interaction force as shown in the figure. Clay platelets are especially smooth and therefore the interaction force will correspond, in the idealized spherical model, to a very low ε parameter. The lower ε, the higher the interaction force.

It is important to highlight that in unsaturated clay soils aggregates are strong units that retain most of the soil water. Soils capable of being compacted in practice have often a certain clay fraction, which is important to ensure the quality of the compacted material. Compaction introduces a certain structure that is in general very different from the conceptual representations of a network of rounded particles of different sizes, a set of menisci at the contacts and, some areas fully saturated with water under tension.

In 1936, Terzaghi stated the principle of effective stresses for saturated soils. This statement implicitly considers the following two hypotheses:

1) The solid particles are incompressible.

2) The contact area between two particles is independent of the confining pressure and can be neglected.

If one of these hypotheses is missing, then different equations can be obtained. For example, if the contact area between particles is considered, the stress regulating the shear strength of soils can be written as [29]

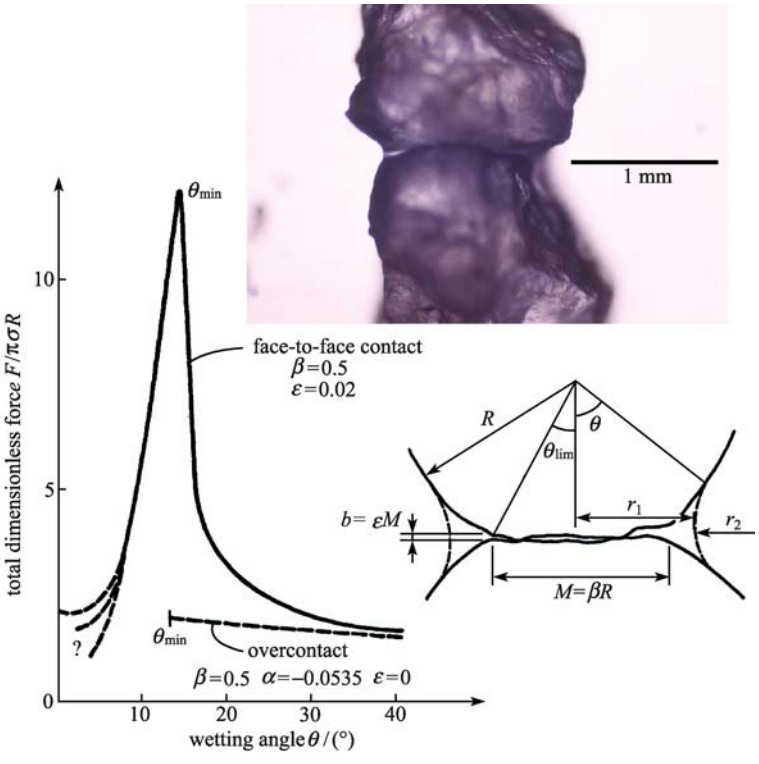

Fig. 18 Capillary forces at planar contacts [28]

$$\sigma' = \sigma - k u_w, \quad (1)$$

where σ' and σ represent the effective and total stress, respectively, u_w is the pore water pressure and k is given by Eq. (2):

$$k = 1 - a\tan\psi/\tan\varphi. \quad (2)$$

In Eq. (2), a represents the contact area between the particles per unit area, ψ is the friction angle of the material of the solid particles and φ is the internal friction angle of the granular media.

On the other hand, according to Ref. [30], the value of parameter k for the volumetric behavior of saturated porous media is given by Eq. (3), where n represents the soil porosity, C_s is the compressibility of the solid material comprising the solid particles and C_e is the compressibility of the soil structure.

$$k = 1 - (1-n)C_s/C_e. \quad (3)$$

The above expressions show that an effective stress does not represent a physical measurable quantity but in fact, it is an artificial stress used to simplify the relations for volumetric and strength behavior of materials and may include some mechanical properties or state variables. However, for the range of stress frequently used in geotechnical engineering, the variation of parameter k is so small that it is very difficult to determine, even with sophisticated equipment. Therefore, Terzaghi's effective stress equation represents a very good approximation for both the shear strength and the volumetric behavior of saturated soils.

Because of this simplification, when researchers were looking for an effective stress equation for unsaturated soils, it was assumed that such equation should account for both the strength and volumetric behavior of the soil and must be written as a function of stress variables. These assumptions, often implicit, gave rise to a great deal of confusion.

Simplifying, there are two main trends to model the behavior of unsaturated soils. The first one, initiated in the middle of the last century, makes use of the effective stress concept. The second one has been developed in the last four decades and uses the concept of independent stress variables.

In the late 1950s, some researchers proposed different effective stress equations [31–34]. However, only the equation proposed by Bishop prevailed because of its simplicity and effectiveness. It is Eq. (4), where u_a is the air pressure and χ a parameter related to the degree of saturation (S_w). The term $(\sigma - u_a)$ is called the net stress (also written σ_{net}) and $(u_a - u_w)$ the soil suction (also written s).

$$\sigma' = \sigma - u_a + \chi(u_a - u_w). \quad (4)$$

The validity of Bishop's equation was questioned from the beginning because it could not predict the phenomenon of collapse upon wetting which occurs when the soil is dried and subsequently loaded above its preconsolidation pressure [35] and finally wetted at constant stress. Bishop's equation predicts the reduction of the effective stress at wetting and this is inconsistent with a soil compression. Based on these results, Burland [36] suggested that the behavior of unsaturated soils could be better understood if the net stress and the soil suction are considered as two independent stress variables. Additional experimental results showed that the value of parameter χ was affected by different factors such as the type of soil, the wetting-drying history, the void ratio and the structure of the soil [35]. These results led to the abandonment of Bishop's equation for many years.

Fredlund et al. [37] performed a stress analysis of an unsaturated soil which was conceived as a four phase system. They concluded, based on a number of triaxial null tests, that the use of two independent stress variables out of three possible combinations of the stresses σ, u_a and u_w were sufficient to describe the stress state of an unsaturated soil. Since then the net stress (σ_{net}) and the soil suction (s) have been the most commonly used independent stress variables. With these variables, Alonso et al. [38] developed a constitutive model for unsaturated soils based on the critical state theory. This model, named Barcelona basic model (BBM), can simulate the phenomenon of collapse upon wetting and was later extended to the case of expansive soils [39]. However, this model did not include the coupling between mechanical and hydraulic behavior that has been experimentally observed in unsaturated soils. Recently, Li [40] proposed a constitutive model based on a thermodynamical analysis, which includes the hydro-mechanical coupling.

The effective stress approach naturally considers the hydro-mechanical coupling of unsaturated soils. However, it is unable to explain collapse effects, as mentioned before. Another objection to Bishop's equation was the consideration that an effective stress relationship should not include state variables (the void ratio or the degree of saturation, for example). However, the "exact" Terzaghi's effective stress equation for saturated soils includes some state variables [29,30]. This means that in fact an effective stress equation represents a constitutive equation.

Some constitutive models based on Bishop's equation have been developed in the last decade (see Refs. [18, 24, 41] for example), adding a separate and independent stress component, essentially related to suction. However, a proper value for Bishop's parameter χ still has not been defined that could be experimentally verified for all the suction range and for both the wetting and drying paths. That is why the value of parameter χ has been customarily equated to the current degree of saturation of the material [42]. However, it is well known that this consideration only represents an approximation to the real value of this parameter. Various authors have proposed different

empirical relationships to define the value of χ [43]. Several researchers have used a thermodynamical approach to propose an effective stress equation for unsaturated soils [44–48]. When considering an isotropic material including the spatial distribution of water menisci, this approach leads to Bishop's equation where $\chi = S_w$. In granular soils the proportion of free water filling macropores is given by the degree of saturation and therefore, the classical Bishop expression is consistent. However, for the case of plastic soils, this equation results in extremely large stresses at low degrees of saturation.

To overcome this problem, Alonso and co-workers [49] consider that an effective degree of saturation should be employed. This parameter defines the proportion of prevailing suction which actually contributes to the effective stress. In that case, the effective stress for unsaturated soils is related to the soil structure and more specifically to the distribution of water in the micro and macrostructure of the soil. The first one is associated with the small pores present in fine soils where water is held by physico-chemical bonds. The second one is represented by the relatively large open pores filled with free water where capillary suction could be applied. In other words, they consider that the microstructure has no contribution on the part of the effective stress generated by suction. Therefore, in the limit case, when the proportion of free water is negligible, the proposed effective stress reduces to the net stress. This proportion of free water can be evaluated from the soil-water retention curves or from porosimetry tests of the material.

These authors propose the following equation to determine the effective degree of saturation:

$$S_r^e = \left\langle \frac{S_r - S_r^m}{1 - S_r^m} \right\rangle, \tag{5}$$

where $\langle \cdot \rangle$ represent the Macauley brackets and S_r^m is the degree of saturation of the microstructure. It represents the immobile water in the soil, or the maximum relative volume of water able to be stored in an adsorbed state.

To allow for a smooth transition between micro and macrostructure the following alternative relation has been proposed:

$$S_r^e = (S_r)^\alpha, \tag{6}$$

where $S_r^e \leqslant S_r$ for $S_r \in [0,1]$ and α ($\alpha \geqslant 1$) is a material parameter. These equations have been tested for several soils regarding shear strength and stiffness. The proposed effective stress provides good predictions. Values found for S_r^e, based on Eq. (6), for a number of soils of varying plasticity and fine's content. Also indicated is the relationship, reported by Jennings et al. [35], between parameter χ of the Bishop equation and S_r for a few materials (compacted clay, compacted shale, a silty clay and two other silty soils, in Fig. 19). Rojas [50] has conducted a similar analysis of the concept of effective stress in unsaturated soil. He relies on previous results by Haines [51], Murray [52] and Desai et al. [53].

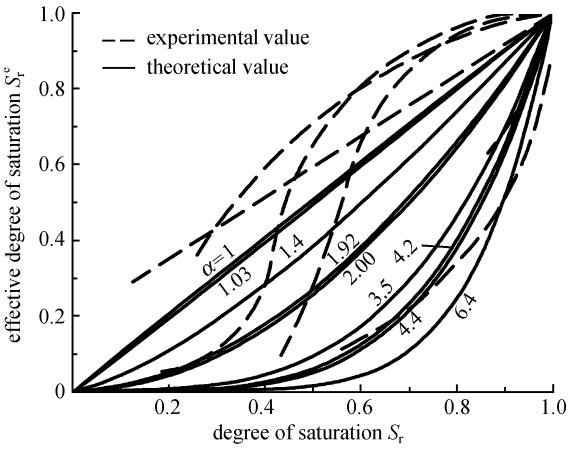

Fig. 19 Theoretical values of parameter χ compared with experimental results by Jennings et al. [35]

3.1.3 Hydro-mechanical coupling

A good example of the coupling between hydraulic and mechanical behavior was presented in Ref. [21]. Two samples of mixture of bentonite and kaolin compacted at the same initial condition (see Fig. 20) were subjected to isotropic loading at constant suction (300 kPa). One of them was previously subjected to a wetting-drying cycle (path *abcd*) while the other was loaded at the compaction water content (path *pq*). Irreversible changes in void ratio and degree of saturation during the suction cycle occurred (see Figs. 20(a)–(d)).

The comparison of the loading curves at constant suction (see Fig. 20(c)) suggests the influence of the previous history of suction on the yielding and plastic compressibility. However, the effect of degree of saturation is difficult to isolate due to the irreversible compression that also occurred during drying. In any case, if a previous wettingdrying cycle leads to a lower void ratio the soil will react by increasing its current yield stress against isotropic loading. A unique virgin loading curve corresponding to the given suction will be reached by both samples according to the model. However, in this case, the experimental data suggested that the apparent preconsolidation stress of the sample previously wetted and dried (which has a lower void ratio and a higher degree of saturation) is slightly lower than the value associated with the sample directly loaded (without a previous suction cycle) (see Figs. 20 (c) and (d)).

In the figures, the virgin compressibility is also different for both samples, the sample with higher void ratio and lower degree of saturation showing higher compressibility. This slight decrease in apparent preconsolidation stress was also observed in other different samples of similar

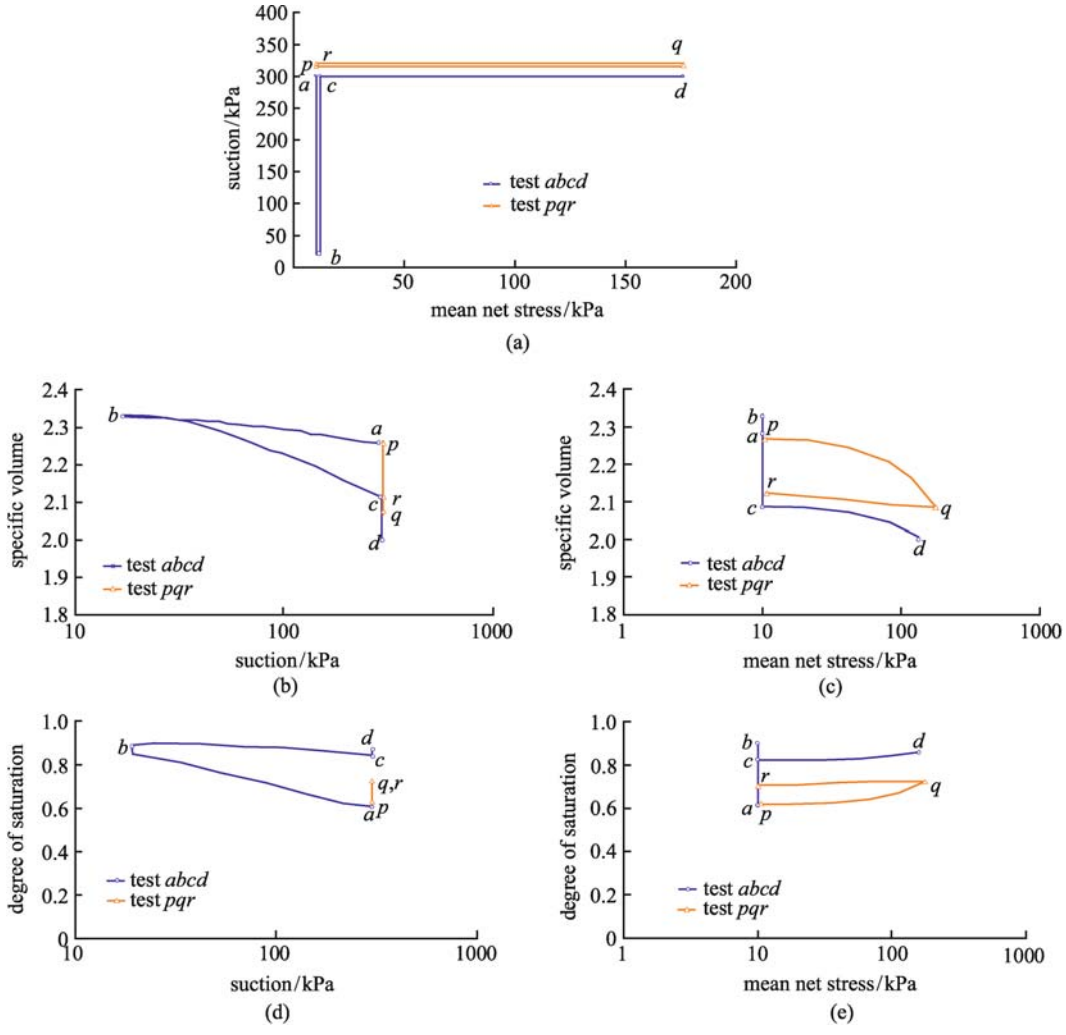

Fig. 20 Specific volume and degree of saturation changes during suction and loading cycles on two bentonite-kaolin samples. (a) Mean net stress: suction; (b) suction: specific volume; (c) mean net stress: specific volume; (d) suction: degree of saturation; (e) mean net stress: degree of saturation [21]

soils by several authors. Additional experimental evidence however is required to characterize these effects in a more conclusive manner for a variety of soil types and initial densities.

Another important aspect of the hydro-mechanical coupling concerns its effects on the shear strength. Increments of shear strength due to drying have earlier been recognized (Refs. [54–61]). However, there is limited experimental evidence for the hydro-mechanical coupling and most cases do not provide the exclusive effect of degree of saturation irrespective of suction effects. Some available experimental data indicate that the critical state for unsaturated states depends on the mean and deviatoric total stress, suction, void ratio and degree of saturation (or water ratio). Vanapalli et al. [62], Vaunat et al. [63] and more recently Tarantino [64] discussed this issue and proposed some strength criteria for different kinds of soils. Experimental results on the effect of previous wetting-drying history and on the effect of degree of saturation are given in Refs. [65] and [66].

The framework proposed by Toll [7,60], to present the experimental data of shear strength behavior provided interesting information of this issue (see Fig. 21). The dependence of the strength with degree of saturation was not attributed directly to the degree of saturation by itself but rather to the fabric of the compacted soil which is affected by this hydraulic parameter: lower degrees of saturation may be able to maintain the presence of aggregation and the soil behaves in a coarse fashion. However, the aggregates will break down at lower values of suction. As suggested also by the authors, the reduced effect of suction at lower values of degree of saturation can be attributed to the reduction in area of water over which the suction acts.

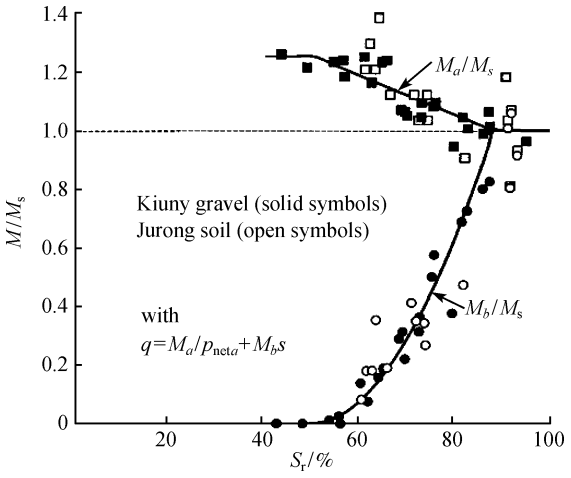

Fig. 21 Normalized functions for critical-state stress ratio with degree of saturation for two soils (M_s is the stress ratio in saturated conditions) [65]

3.1.4 Types of soils and the effect of suction

Figure 22 is a representation of the particle sizes of a few types of soils proposed in Ref. [3], previously mentioned. The materials selected (shale rockfill used to build Lechago Dam, sand from Castelldefels beach, Barcelona clayey and sandy silt and Febex bentonite) can be considered to be representative of each soil type. The figure shows only the ranges of particle sizes for each case.

Grain size provides limited information. Since unsaturated soil mechanics deals with the role of water (partially) filling the pores, the analysis of the pore size distribution of the soils is more useful. Mercury intrusion porosimetry tests provide this information, covering void diameters ranging from 10^{-6} mm to 1 mm. Data from this test provides information on soil structure: fine soils and mixtures of fine soils with granular materials usually exhibit a bimodal structure which consists of a microstructure and a macrostructure [67,68] and clean uniform granular soils exhibit a single structure (a single peak in the predominant dimension).

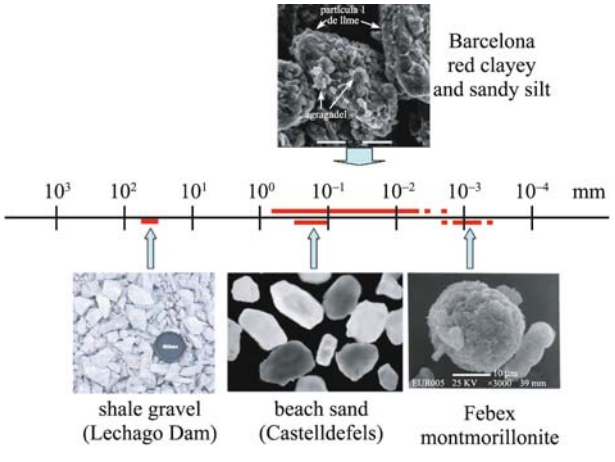

Fig. 22 Grain size of several soil types [4]

Figure 23 presents different pore sizes in compacted Boom clay detected by MIP. The change induced by a wetting and drying cycle is shown. The microstructure is formed by packets of fine particles that flocculate and become stiff when dry. These packets or aggregates produce the intra-aggregate pores which are pores of small size. On the other hand, the macrostructure results from the arrangement of the packets or aggregates. Inter-aggregate pores are pores of larger size. The effect of a suction cycle will be analyzed further in the paper.

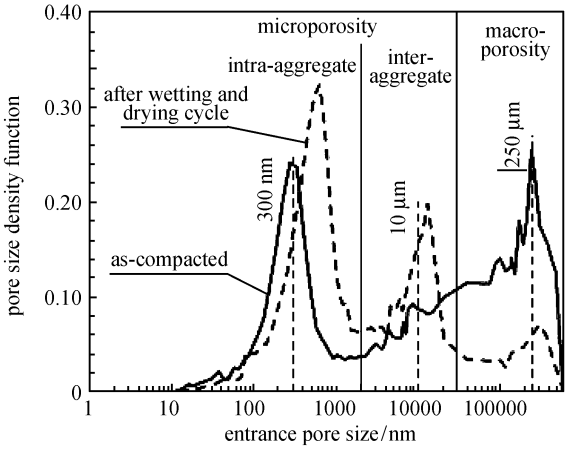

Fig. 23 Different pore sizes [67]

MIP, water retention properties (through the WRC) and volume changes measured in swelling tests (tests performed in oedometric cells where samples are fully saturated under different vertical stresses) provide useful information on the hydro-mechanical behavior of the different soil types. In fact, these differences are what justify the need of defining different soil types.

Castelldefels beach sand shown in Fig. 22 is a uniform material (C_u= 1.8) whose grains vary between 75 μm and 500 μm in size. Samples were prepared by pluviation to the minimum density. MIP shows monomodal and symmetric distribution of pores around a dominant entrance pore size, as expected. The WRC is conceptually simple because the sand remains saturated for low suctions and it is easy to identify the air entry value, which is the value of suction for which the soil loses most of its pore water. For suctions above this value, water is stored at the contacts between particles in the menisci. Loose specimens (e = 0.95) prepared at the hygroscopic humidity were subjected to collapse tests in a suction controlled oedometer cell. Collapse was measured upon partial wetting and increased significantly in a final wetting stage close to saturation. However, the absolute value of collapse strains was quite low.

The Barcelona clayey and sandy silt from Fig. 22 (sand: 39.4%; silt: 44.5%; clay: 16.1%) classifies CL (w_L= 32%; w_P= 16%). Specimens were statically and isotropically compacted (in a triaxial test) at different confining mean stresses (in the range 0.3–1.2 MPa) [20]. Three dry densities were analyzed to study density effects on the hydro-mechanical properties of the material. Bimodal pore size distribution curves from MIP were identified and are shown in Fig. 24(a). The peak observed at the larger diameters, corresponding to the dimensions of the large pores, depend on dry density. It was concluded that changes in void ratio are essentially associated with the large pores.

The smaller macropores of the denser samples explain the smaller saturated water content identified in the WRC shown in Fig. 24(b).

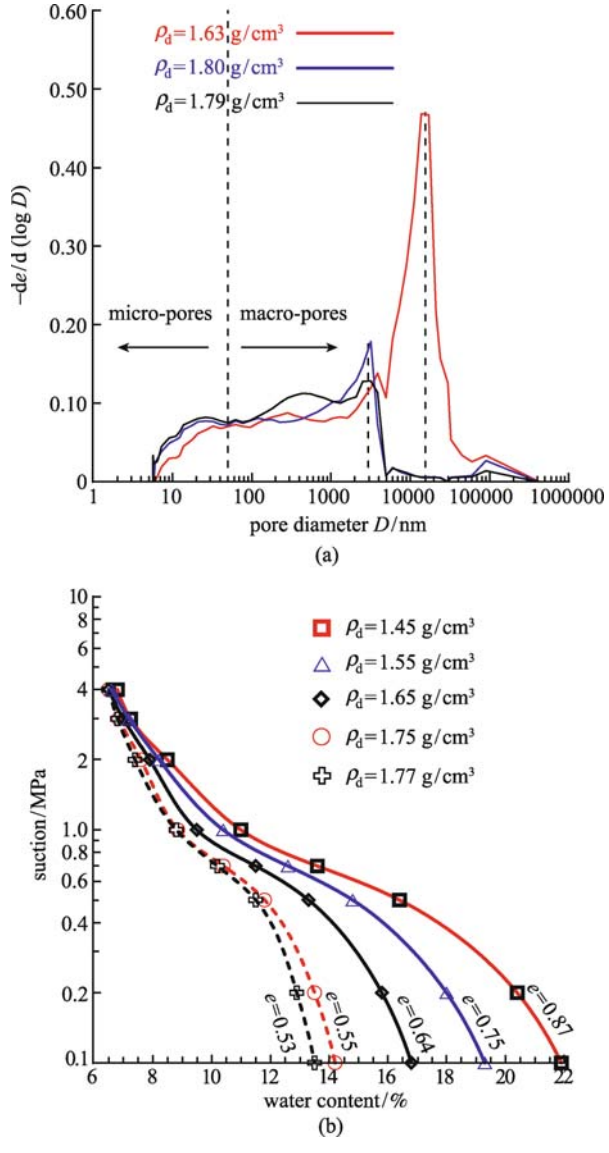

Fig. 24 Barcelona red silty clay compacted at different dry densities. (a) Pore size distribution curves; (b) WRCs [20]

In an idealized granular soil constituted by relatively big particles and (saturated) clay packets or aggregates, the degree of saturation associated with the free water in the macropores is effectively controlling the mechanical behavior of the soil [11,13,15]. At a given suction, water is filling some voids (bulk water) and it is also present in the form of menisci at the inter-particle contacts around air-filled voids. The hydro-mechanical coupling implies that the stress acting on the soil skeleton has two components: A component of stress transmitted through the skeleton, which is influenced by the suction of bulk water (basically in the same way of pore water in saturated soils) by means of normal and tangential forces acting on particles contacts; and a second component which corresponds to an internal stress induced by the capillary stress in the menisci. This second component provides an additional bonding effect essentially by means of normal forces between particles [24,69–71]. Gallipoli and co-workers [24] assumed that the bonding meniscus enables the soil skeleton to sustain a void ratio higher than that corresponding to the saturated soil at the same average skeleton stress. Theoretical analyses on the effect of suction on the unsaturated behavior have been published by several authors [26,47,72,73].

These considerations of the double effect of suction, depending on the arrangement of water in voids, suggest that not only the suction will affect significantly the mechanical response of a soil but also that the proportion of the soil over which different suction mechanisms acts is relevant [24]. Probably the degree of saturation is the most adequate parameter incorporating such information [26,74]. Irreversible compression caused by suction cycles shown by several authors [8,16,21] proves this idea.

Figure 18 previously presented supports the idea that capillary action (the force system associated with menisci at grain to grain contacts) is suitable to explain the changes of macroporosity as a consequence of the rearrangement of grains or aggregates.

Within the aggregates in clayey soils, however, water is adsorbed by electrochemical forces and capillary notions are not directly applicable. The narrow space between clay platelets may effectively act as a “semipermeable membrane” preventing the free access of ions. Therefore, osmotic potentials as well as the classical capillary or “matric” potential will control the deformation of aggregates. Therefore, it has been suggested [16] that the total suction will control the behavior of clay aggregates.

Clayey soils exhibiting a double structure such as the Febex bentonite, included in Fig. 22, will exhibit a complex behavior, derived from the interaction between the micro-structure and the macrovoids. Coarser materials (coarser sands and gravels) should not react to changes in water content. A good reason for this expected behavior is that capillary forces at grain to grain contacts become exceedingly small if compared with stress or self weight induced granular forces. This is the case for coarse sands, a

very stable material, not sensitive to changes in water content, and rockfill. The WRC typical of these materials shows a large saturated water content associated with the large dimensions of the voids between the grains and a well marked air entry value.

However, if the size of grains increases towards gravels and rockfill sizes, the engineering experience in structures such as rockfill embankments and dams is that wetting leads to settlements. Rockfill deformation upon wetting, once it is confined under stress, has been explained by the rupture of individual particles. In a recent series of papers the particle breakage mechanism has been investigated in more detail [75–78]. It turns out that the relative humidity (or, alternatively the total suction) of the "atmosphere" filling the large voids between rockfill particles controls the stiffness of coarse grained materials. This is an interesting result because water suction maintains a key role for volumetric changes at the large scale but the basic deformation mechanism is now totally different. Oldecop et al. [76] indicated that the role of the total suction is to control the speed of crack propagation within individual rockfill particles. This is a "new" mechanism, not present in soils. It is as if water would act as a corrosive agent, as will be explained when rockfill materials are analyzed. The deformations observed in these materials are therefore related with structural changes caused by the rearrangement of the fragments resulting from a breakage process.

From the discussion presented it can be concluded that unsaturated soil mechanics explain the different behavior of each type of unsaturated soil proposed because it considers the hydraulic and mechanical coupling inherent to the different sizes of the particles or clay aggregates, their chemical nature and their spatial arrangement (density, void volume and saturation degree). The two mechanisms described, the first observed in compacted soils involving capillary effects and eventually osmotic effects, and the second observed in rockfill materials, where suction is related with breakage, are very distinct. The two mechanisms can be seen as extreme cases of behavior and are typical of special types of soils. Compacted soft rocks on the other hand, share properties of both types of simpler behavior. They will be discussed in Section 3.2

3.2 Unsaturated constitutive models

3.2.1 Regular compacted soils

Compaction basics

In this section the behavior of a reference compacted material is discussed. BBM, previously mentioned [38], is taken as a reference because this constitutive model is able to reproduce the main features of behavior of compacted non-expansive soils. However, expansive clayey soils are treated differently and require more sophisticated models because volume changes of the microstructure also affects mechanical behavior.

In the final part it is discussed how the values from compaction tests can be used to find BBM parameters. Basically, the idea is to replace the pair (γ_d, w), which identifies a state of compaction, by the stress pair (p_0^*: isotropic yield stress for saturated conditions; s: suction). Identifying this correspondence can be a relatively simple task for non-expansive materials but it is not so for materials where microstructure shows important volume changes caused by stress and suction paths. This observation suggests that material parameters are also controlled by the compaction state.

The process of compaction of clayey or silty soils tends to produce a distinct double structure. This is a consequence of the tendency of clay particles to pack together in units of low porosity. These units, the aggregates, behave as grains, especially if they are rigid (high suction) leaving among them larger pores (macropores). Changes in porosity, quantified by dry density changes, are mainly accommodated by changes in macroporosity. This was shown previously in Fig. 23 for low expansive clays. Note also that the macropores of very active clays may be as big as the pores of uniform sand.

Differences in pore size distribution induced by the compaction water content are shown in Fig. 25 for Barcelona silty clay statically compacted under 0.6 MPa [79]. The samples have the following meaning: 1) DD: samples compacted on the dry side; 2) WW: samples compacted on the wet side. Compacting on the dry side induces a significant proportion of bigger pores which are absent in the samples compacted on the wet side.

Compacting on the dry side tends also to introduce a network of large macropores, if compared with optimum (or wet of optimum) compaction. The denser the specimen the smaller the average diameter of (macro) pores. The

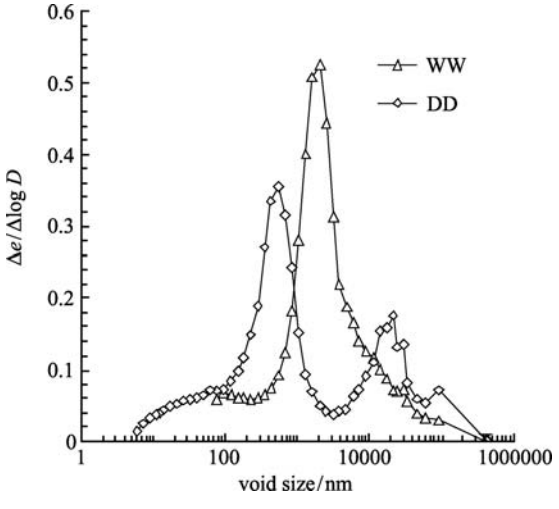

Fig. 25 MIP for Barcelona red silty clay compacted in the dry and wet side [79]

type of macrostructure affects the volumetric changes of the material when fully saturated. Different samples of Barcelona silty clay were compacted at different dry densities and water contents. Several states in the plot (water content: dry density) were tested. The samples were fully saturated under 0.1 MPa vertical stress in oedometric conditions and strains measured. Figure 26 presents the curves for equal swelling and collapse strains measured in the tests. The curves show that volume changes depend on the soil density and the initial suction. The optimum value for standard Proctor compaction is also identified in the figure. Swelling strains for this point are practically zero, which can be explained by a stable structural configuration.

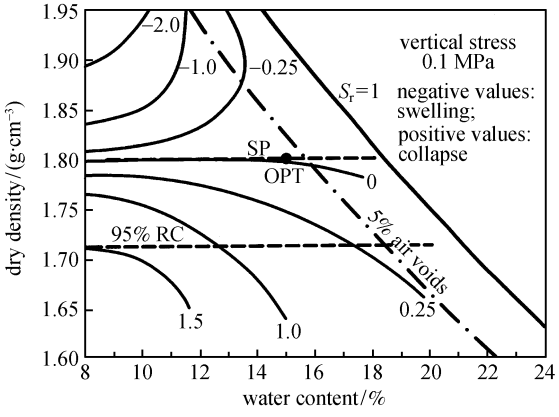

Fig. 26 Equal swelling deformation curves measured in samples of Barcelona red silty clay [79]

Any compacted soil may experience expansion when wetted from an initially unsaturated state. However, the effect of the confining stress should be considered also. This effect is illustrated in Fig. 27. In this figure, the volume changes expected for different densities (dry of optimum) are related with vertical stress. The type of soil (mineral constituents and its density) determines the threshold stress that marks a swelling-collapse transition. On the other hand, the higher the density and suction, the higher the swelling strain for a given confining stress

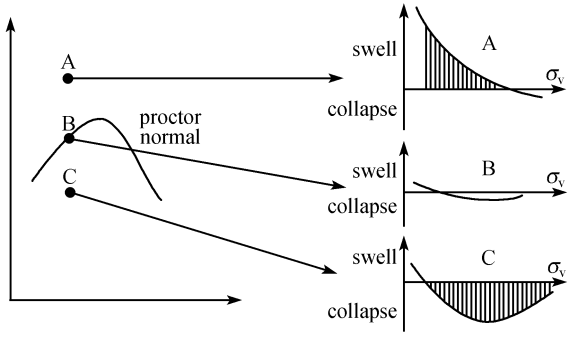

Fig. 27 Schematic representation of volume changes upon full saturation experienced by compacted soil

(provided it is low enough to allow swelling). Therefore, collapse and swelling are opposite phenomena for a continuously varying behavior, which, other conditions being equal, depend on the confining stress.

As mentioned previously, water content and dry density are related with suction. Therefore, suction is a continuously varying function when plotted in a (γ_d, w) plane (Fig. 28 for Barcelona silty clay). The different volume changes can also be explained by different suction changes experienced by the material upon full saturation.

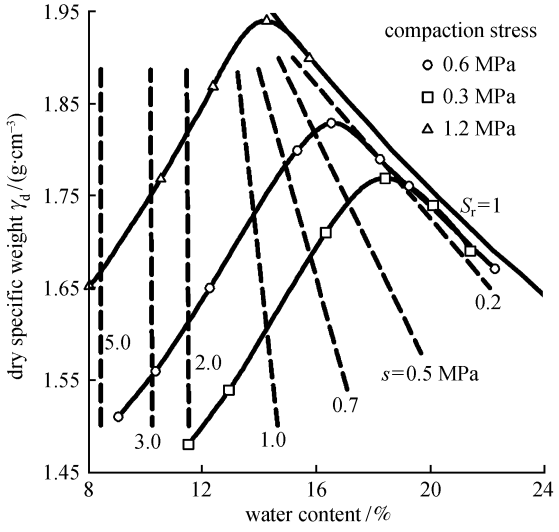

Fig. 28 Static compaction curves of Barcelona silty clay and contours of equal suction [79]

The shape of the compaction curve generally depends on the compaction procedure [4]. It is different if the soil is compacted dynamically and statically. The dynamic compaction curve has a clear maximum density unlike the curve obtained by static compaction. Static compaction, which involves comparatively smaller shear straining than dynamic compaction, induces the aggregation of clay particles even for compaction on the wet side.

It can be concluded that the initial state of the compacted soil is defined by the initial dry density/void ratio, by the initial suction/water content and by the compaction process. It is expected that this state would have to be considered in the definition of the constitutive model.

Most of the theoretical developments made in recent time concern the behavior of medium to low plasticity soils. In addition, most of the experimental research is essentially based on statically compacted soils or clays of low plasticity and high porosity.

BBM

BBM is an elastoplastic constitutive model where suction, s ($s = u_a - u_w$, with u_a the air pressure and u_w the liquid pressure), is a state variable besides mean net stress, p (defined as the excess of mean stress over air pressure)

and specific volume, v (for the reproduction of volumetric behavior).

According to BBM, two yield surfaces limiting the space where the soil behaves elastically are defined in (s:p) space: the loading collapse (LC) yielding curve and the suction increase (SI) curve. Both are presented in Fig. 29. Also indicated in the figure is the volumetric response measured by specific volume v of the model against some suction-stress paths.

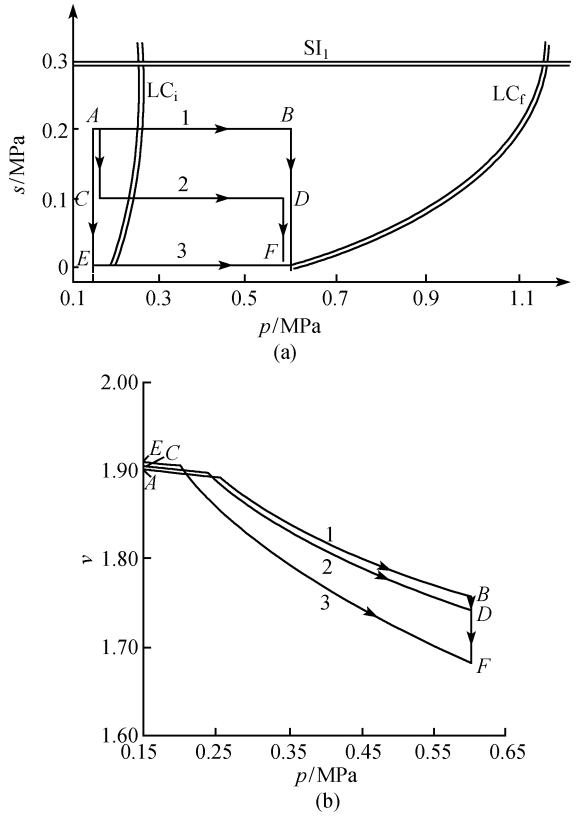

Fig. 29 Barcelona basic model. (a) Elastic space defined by SI and LC curves in space (s:p); (b) volumetric deformations for different stress paths [38]

BBM requires the following set of material parameters to be applied: elastic behavior (isotropic): κ, κ_s (compressibility coefficients against mean net stress and suction changes); volumetric behavior (plastic states): $\lambda(0)$ (virgin saturated compressibility); β (MPa^{-1}) and r defining the LC yield curve; k, G (MPa), M defining shear behavior and strength and a reference stress parameter p^c (MPa). p^c is a reference pressure which enters into the definition of the yield curve LC:

$$\frac{p_0}{p^c}=\left(\frac{p_0^*}{p^c}\right)^{\frac{\lambda(0)-\kappa}{\lambda(s)-\kappa}}, \tag{7}$$

where p_0 and p_0^* are the current isotropic yield stresses for suction s and for saturated conditions. $\lambda(s)$ defines the volumetric compressibility for suction

$$s(\lambda(s)=\lambda(0)[(1-r)\mathrm{e}^{-\beta s}+r]).$$

It was proposed to locate p^c in a position which satisfies Eq. (8), where $N(0)$ and $N(s)$ are the specific volume of the soil under 1 MPa for suctions s and 0, respectively.

$$N(0)-N(s)=\kappa_s\ln\frac{s+p_{atm}}{p_{atm}}. \tag{8}$$

The isotropic description of BBM requires six constitutive parameters: p^c, $\lambda(s)$, κ, κ_s, r and β. The last five parameters have a physical meaning. However, parameter p^c is more difficult to define in practice. Its definition through Eq. (8) was simply a matter of convenience in order to arrive at a compact and simple expression for the yield locus LC (see Eq. (7)). If p^c is accepted as a constant parameter then the modeled (real) soils should behave in a specific manner, and, in particular, for any suction s the corresponding isotropic virgin compression line should provide a unique value of p^c (through Eq. (8)). This is unlikely, however.

Alonso et al. [4] proposed other alternatives. Assume for instance that the virgin compression lines cross in a single point defined by a specific volume N_n and a confining stress p_n. Some test results seem to support this behavior. This feature is not covered by BBM, but a modified version can be easily derived if (N_n, p_n) are taken as a reference point to locate the position of virgin compression lines. Then, it can be shown that the new equation of LC is

$$\frac{p_0}{p_n}=\left(\frac{p_0^*}{p_n}\right)^{\frac{\lambda(0)-\kappa}{\lambda(s)-\kappa}}\left(\frac{s+p_{atm}}{p_{atm}}\right)^{\frac{\kappa_s}{\lambda(s)-\kappa}}. \tag{9}$$

This can be considered a modified BBM . Now, instead of p^c, the reference stress values is p_n. In this case there is no uncertainty in its determination, because of the assumption, previously made, that all virgin compression lines cross at a unique point. Any pair of compression lines would now provide a unique value of p_n. With this modification all parameters will have physical meaning and therefore they can be estimated from tests.

The isotropic formulation of BBM was extended to triaxial states by means of ellipses that span the p axis from a value $p_s=ks$ (which provides a linear increase in cohesion with suction) to the LC curve. Two additional parameters were required, the elastic shear modulus, G, and the slope of the critical state line, M. The yielding surface for triaxial states is presented in Fig. 30.

BBM reproduces the following behaviors:

1) Yielding stresses increase with suction.

2) Final state is always in the saturated normal compression line when collapse occurs after full saturation.

3) Several wetting paths observed in real cases can be

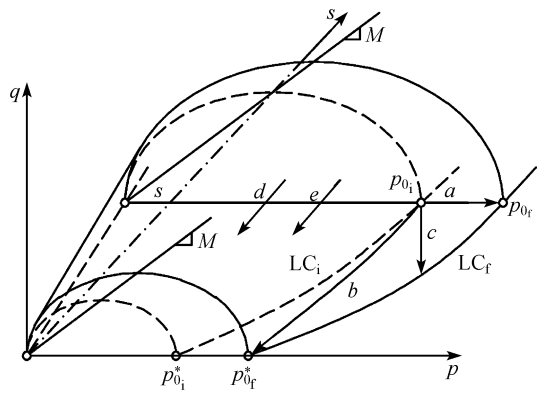

Fig. 30 Yielding behavior (triaxial states) of BBM

reproduced (pure swelling, swelling followed by collapse, Monotonic collapse if the initial soil state is on LC).

4) Shear strength increases with suction.

5) The model follows critical state conditions for constant suction.

6) In swelling pressures tests (wetting at zero volume change) it may predict a maximum of swelling pressures for some intermediate value of suction (when the stress-suction path touches LC) or a monotonic increase in swelling pressure if the stress path is entirely within the elastic range.

BBM has a number of limitations that would become clear when other developed soil models are reviewed. To summarize, it is not coupled with hydraulic effects (suction has to be independently related with water content and stress state); it is not appropriate to describe expansive soils (in particular swelling strains are not prevented by confining stresses within the elastic region); it does not consider anisotropy (inherent or induced) by the applied stress path and it includes also the limitations of modified Cam-clay (hardening is isotropic and volumetric, no kinematic hardening, inaccurate representation of yield locus for high OCR's). It does not consider either some advanced features found in constitutive models for saturated soils (small strain behavior; ability to model cyclic application of stress; creep effects, etc.).

The comparison between BBM predictions and the behavior observed for expansive soils shows that the model is inadequate in the following aspects:

1) Swelling and collapse deformations are not controlled by the state of compaction (initial density) (see, however, Fig. 26).

2) In BBM swelling is elastic and depends only on initial and final suction but, in reality, swelling deformations depend on the loading path followed (stress and suction changes).

3) BBM cannot reproduce the accumulation of plastic deformations with increasing number of suction cycles.

In view of these limitations the BBM was modified to accommodate the behavior of expansive soils.

Expansive soils. BExM

Gens et al. [39] considered that the elastic space on the (p, s) plane was limited by a new yield locus (SD, after suction decrease). When unloading or wetting of the soil takes place and the stress path reaches SD, irreversible expansive strains occur. They are further controlled by the relative positions of SD and LC. This introduces naturally a dependence on current void ratio or dry density. LC and SD are coupled through the plastic volumetric strain rates. Paths along SD are "neutral": they do not induce microstructural volumetric strains. They correspond to swelling pressure tests.

In the original BExM two structure levels are defined: the microstructure, composed by clay and other minerals (aggregates), and the macrostructure (the overall structure). More levels can be considered, depending on the relevance of the deformations at each level and the particularity of the case [80]. The most important factor in this model is the definition of the interaction between the structural levels considered. The idea behind the model is that the volumetric deformations of the clay minerals (microstructure) ($\delta\varepsilon_m$) affect global behavior in an irreversible manner. Assuming that the deformations of the microstructure are elastic, the plastic deformations are the deformations of the macrostructure ($\delta\varepsilon_M^P$).

Because the water at the microstructural level can be considered water from mineral constitution, it is acceptable to assume that the clay aggregates are saturated independently from overall suction. The behavior of the macrostructure, or clay matrix, is assumed to be ruled by stress and suction changes. Therefore, BBM or a similar unsaturated soil constitutive model can be used to describe it. BBM was the model chosen in the original formulation. It is assumed that macrostructural plastic deformations are independent of their origin since they are calculated by the hardening rules adopted (displacement of the LC curve). In the model, the behavior of the microstructure is totally independent of the behavior of the macrostructure. This is an advantage because different models can be adopted to make BExM more appropriate to reproduce some particular features of behavior, as will be explained later in this section.

Figure 31 presents the yielding surfaces in (p:s) space considered in BExM. From the macrostructural point of view, plastic volumetric deformations can be caused by stress increment or by saturation (collapse), as soon as the loading-collapse yield curve (LC curve defined by BBM) is crossed.

The contribution of the microstructure to the calculation of the plastic deformations is accounted with the neutral line curve (NL curve in Fig. 31(a)). NL corresponds to microstructural constant volume during loading since the saturated effective stress ($p' = p + s$) is kept constant (the slope of NL is 45° in Fig. 31(a)). During wetting, from point A to B in Fig. 31(a), if the curve NL is crossed the

microstructural swelling deformations will affect the macrostructural arrangement. It also defines a yielding surface in the sense that macrostructural plastic deformations will be developed.

The coupling between the two levels is simulated by an interaction function (also named coupling function) calibrated to fit experimental data (see Fig. 31(b)).

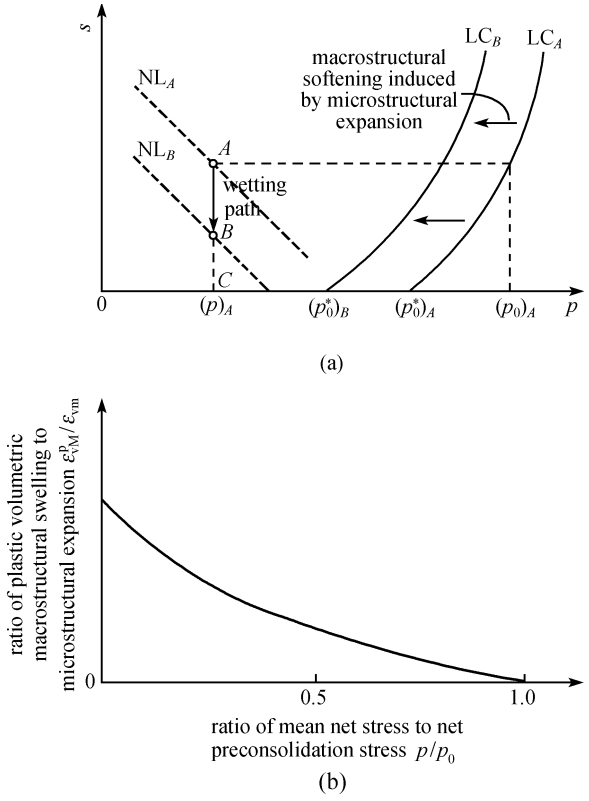

Fig. 31 BExM. (a) Yielding surfaces in (p:s) space; (b) interaction function f (suction decrease) [39]

The final deformation of the macrostructure depends on the density of the clay besides the intensity of its deformations, because the effects of microstructural swelling depend on the macrostructural rearrangements required to adapt to these deformations. A simple way to represent the density of the clay is by relating the current mean net stress level, p, with the preconsolidation value, p_0. A value of p/p_0= 1 indicates a very open macrostructure (the soil is in the virgin compression line), almost insensitive to swelling of the microstructure. In this case, a potential collapse situation may be expected due to microstructural swelling instead of global swelling, therefore, the interaction function f must be zero. Decreasing values of p/p_0 imply increasingly denser packings of the macrostructure (increasing values of p_0). The stress level is also considered since the confined macrostructure is becoming insensitive to microstructural deformations for increasing values of p/p_0.

Alonso [81] proposed a modification to the model that allowed simulating suction cycles and different types of macrostructural deformation. The model is presented in Fig. 32(a). Two yielding curves were introduced replacing curve NL; curves suction increase (SI) and suction decrease (SD), corresponding respectively to shrinkage and swelling of the clay minerals. They limit the interval for which the volumetric deformations of the microstructure do not affect irreversibly the macrostructure. As for the curve NL, these two curves correspond to constant volume during loading since saturated effective stress (p'= $p + s$) is kept constant.

Two different interaction functions are defined, f_D and f_I, corresponding to curves SD and SI (see Fig. 32(b)). The macrostructural plastic volumetric deformation, $d\varepsilon^p_M$ (ε^M in Fig. 32(b)) is given by Eq. (10) [81] when curves SI or SD are mobilized. In this equation, $d\varepsilon_m$ (ε^m in Fig. 32(b)) is the deformation of the microstructure, and f_{D0}, f_{I0}, f_{D1}, f_{I1}, n_D and n_I are constants calibrated to fit experimental data (I for suction increase function, f_I, and D for suction decrease function, f_D).

$$d\varepsilon^p_M = \begin{cases} d\varepsilon_m f_D = d\varepsilon_m \left(f_{D0} + f_{D1} \left(1 - \dfrac{p}{p_0} \right)^{n_D} \right), \\ d\varepsilon_m f_I = d\varepsilon_m \left(f_{I0} + f_{I1} \left(1 - \dfrac{p}{p_0} \right)^{n_I} \right). \end{cases} \tag{10}$$

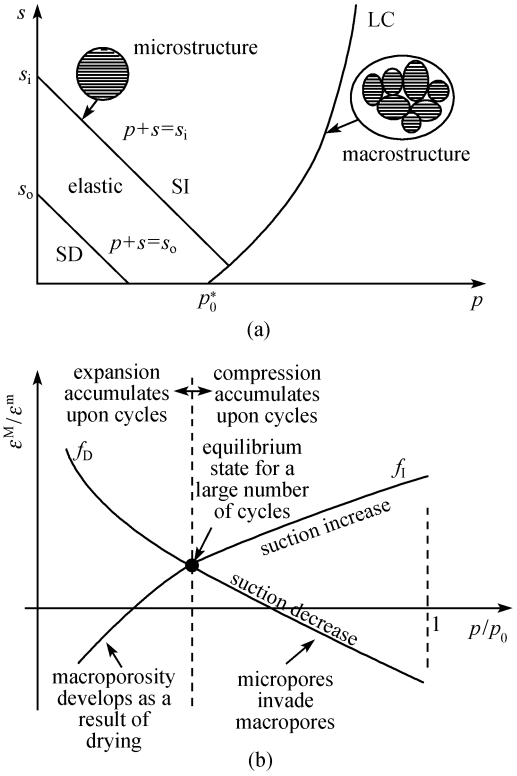

Fig. 32 BExM adapted to include suction cycles. (a) Yielding surfaces in (p:s) space; (b) interaction functions suction decrease (f_D) and suction increase (f_I) [81]

Adopting BBM as constitutive model for the macrostructure, the plastic volumetric deformation when curve LC is mobilized is calculated with Eq. (11):

$$d\varepsilon_M^p = -\frac{\lambda_M - \kappa_M}{1+e_0}\ln\left(\frac{p_0}{p_y}\right). \quad (11)$$

The macrostructural elastic volumetric deformation $d\varepsilon_M^e$ is given by Eq. (12). The constants in Eqs. (11) and (12) have the following meaning: e_0 is the initial void ratio, p_0 is the saturated mean isotropic net yielding stress before loading, p_y is the saturated mean isotropic yielding net stress after loading, λ_M is the compressibility parameter for changes in mean net stress for virgin states of the soil, κ_M is the elastic compressibility parameter for changes in mean net stress and κ_s^M is the elastic compressibility parameter for changes in suction.

$$d\varepsilon_M^e = -\frac{\kappa_M}{1+e_0}\ln\left(\frac{p}{p_0}\right) - \frac{\kappa_M}{1+e_0}\ln\left(\frac{s}{p_{atm}}\right). \quad (12)$$

For the microstructure, assuming elastic behavior and full saturation, the volumetric deformations $d\varepsilon_m$ are given by Eq.(13), where p' and p_0' are the current and yielding saturated mean isotropic effective stresses, respectively, and κ_m is the elastic compressibility parameter for changes in mean effective stress.

$$d\varepsilon_m = -\frac{\kappa_m}{1+e_0}\ln\left(\frac{p'}{p_0'}\right). \quad (13)$$

The model [80,82] was used to explain the accumulation of plastic deformations during cyclic suction tests performed on samples of compacted expansive clays. This can be achieved by mobilizing in alternate manner the interaction functions f_I (drying path) and f_D (wetting path), which imply changes on the yielding stress p_0, simulating hardening on drying and softening on wetting.

The calibration of the interaction functions can be adapted to several cases. The different signs of the interaction functions have also physical meaning: when positive, the volume changes of the microstructure and of the macrostructure have the same sign (global shrinkage caused by microstructural shrinkage, global swelling caused by the swelling of the microstructure); when negative the signs of the volume changes are opposite (global collapse shrinkage caused by microstructural swelling, microstructural swelling invading the macropores). Figure 33 illustrates some possible structural rearrangements due to the volume change of the microstructure caused by suction changes. In the figure, the clays are represented in a simplified manner by stacks of parallel platelets.

BExM is able to predict continuing plastic strains during wetting-drying cycles. By suitable choice of the coupling relationships between the macrostructural plastic strains and the microstructural elastic strains, it is also possible to predict that the behavior will shake down to a stable hysteretic loop after a few cycles [82].

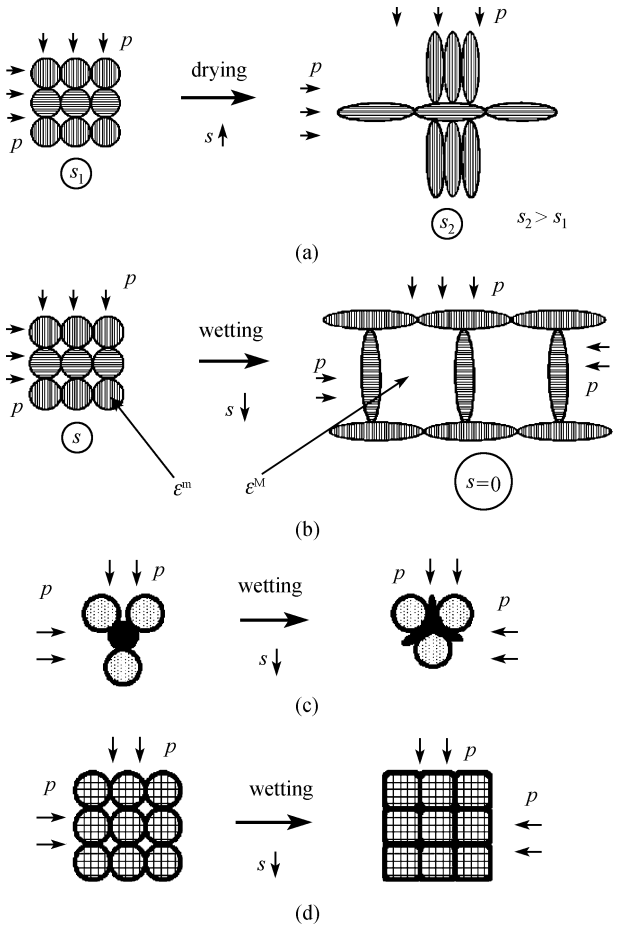

Fig. 33 Some possible macrostructural deformations (ε^M) caused by the deformations of the microstructure (ε^m) under suction changes. (a) Drying: shrinkage of clay eventually with global volume increment (f_I negative); (b) wetting swelling of clay eventually with global volume increment (f_D positive); (c) wetting: loss of stiffness of clay eventually with global volume decrease (f_D negative); (d) wetting: swelling of clay invading macropores eventually with global volume decrease (f_D negative) [82]

Based on the elastoplastic framework established by BBM, several models were developed in the following years improving some shortcomings of the basic model and/or including additional new constitutive relationship. One of the main modifications was the inclusion of hydraulic coupling, for example (see Refs. [83–85], among others). Their review is out of the scope of this paper.

The characterization of compacted states

Compaction states are defined in practice by dry density (γ_d) and water content (w). A close relationship between the two sets of variables, (γ_d, w) and (p_0^*, s), is likely to occur. This is because it is assumed that BBM could be taken as a reference acceptable model for compacted soils, at least for a limiting range of confining stresses.

In BBM, the initial state of the soil is characterized by two stress variables: suction (s), and isotropic yield stress for saturated conditions (p_0^*). Suction is related, through WRC, to water content and void ratio (or dry density). On the other hand, if the static compaction process is represented as a virgin loading, starting at a loose state, there will be a direct relationship between the attained void ratio (or γ_d) and the maximum stress applied, i.e., the preconsolidation stress.

The LC curve relates all the preconsolidation states with the saturated state through a number of constitutive parameters. It may be expected that p_0^* and γ_d are closely related. This characterization of compacted states in terms of (p_0^*, s) was discussed by several authors [83,86–89]).

LC curves have been found and published for a number of different compacted soils. One example is given in Fig. 34 (Boom clay; see Ref. [15]).

Values of p_0^* have been collected from this and a few other sources [4] and plotted in Fig. 34 as a function of the dry density of the specimen tested. p_0^* increases exponentially with γ_d. The plot in Fig. 35 shows the different soils ordered in the sense of their plasticity: the higher the plasticity the higher p_0^*, for a given dry density. Most probably the degree of uniformity of the grain size distribution controls also p_0^*, for a given dry density and plasticity. This plot may help to find a suitable initial p_0^* value when only standard compaction tests are available.

Given a particular soil, if the initial compaction state dominates the subsequent mechanical behavior, models such as BBM offer a simple and powerful procedure to represent compacted soil behavior. A unique set of material parameters ($\lambda(0)$, β, r, κ, κ_s, p^c) will characterize the soil mineralogy and grain size distribution. Initial compaction states will be described by (p_0^*, s). Sensitivity analysis, for instance, will be facilitated in such a scenario. However, if

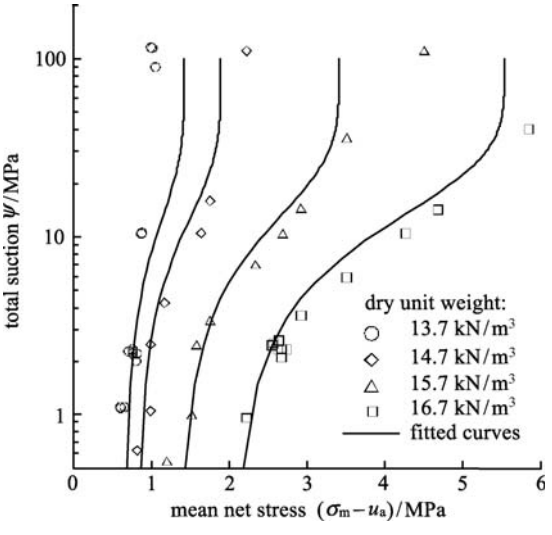

Fig. 34 LC yield surfaces of statically compacted Boom clay [15]

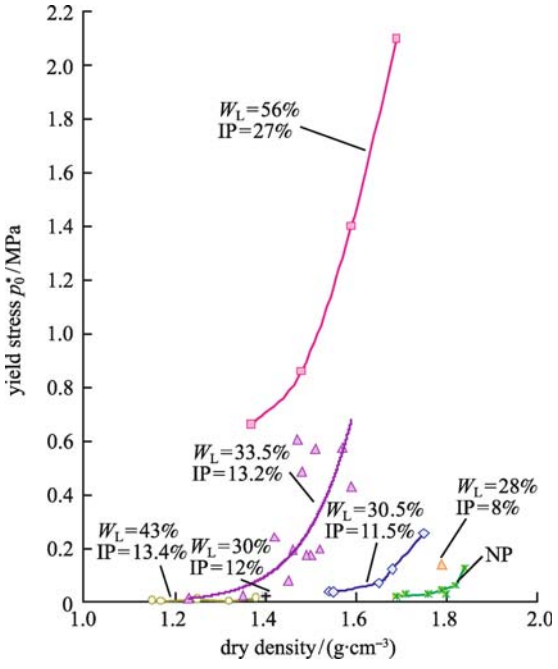

Fig. 35 Compaction and yield stress [4]

varying compaction conditions introduce "fundamental" changes in the sense of modifying the set of constitutive parameters (one reason may be that soil microstructure changes fundamentally across the compaction space) a more complex picture emerges.

A number of testing programs were reviewed in Ref. [81] having this idea in mind. It was concluded that for some soils the implicit framework outlined could provide a good representation of soil compaction. This implies that the microstructural differences found in a compaction plane, not accounted for by changes in void ratio, are relatively unimportant. However, it was also found that in some soils this simple framework was insufficient. Further discussion on this topic is given in Refs. [61,88,89]. Sivakumar et al. [88] interpreted some triaxial test on statically compacted speswhite kaolin and found that the slope and intercept of normal compression lines would be a function of water content and compaction stress. The slope and intercept of the critical state line was found to depend only on compaction water content.

Tarantino et al. [61,90]) tested also statically compacted speswhite kaolin in suction controlled oedometers. They found a unique compression boundary surface which is reproduced in Fig. 36. The representation uses a Bishop type effective stress and a reduced suction (ns) for the two "stress" axis.

This discussion is not independent of the conceptual constitutive model used to reproduce compacted soil behavior. If soils models become more sophisticated, chances to reproduce compacted soil behavior with a common set of material parameters probably increase.

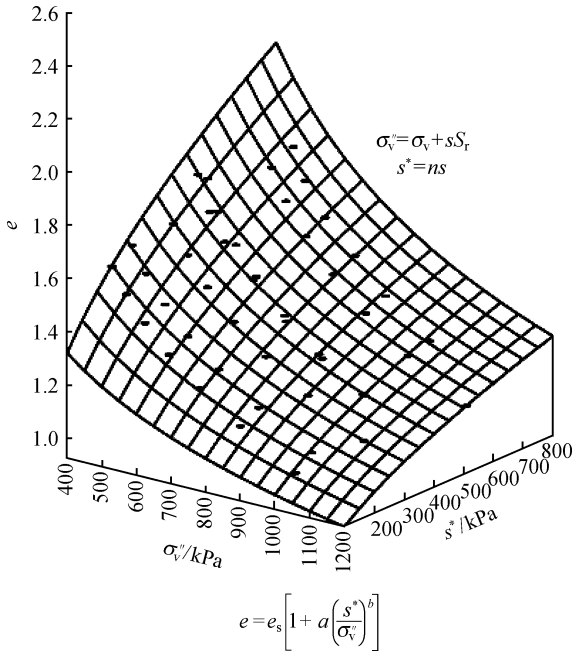

Fig. 36 Virgin compression boundary surface derived from oedometer tests on statically compacted speshwhite kaolin [61,90]

One particularly relevant aspect in this topic is the compacted soil microstructure, which was mentioned previously in the analysis of MIP plots for expansive and non-expansive clays. Changes in microstructure (as exemplified by the pore size distribution) are not included in changes of void ratio. Therefore, the simple framework described will have always some limitations when microstructure is important. One possibility is to modify some constitutive parameters and to relate them to the initial compaction state. Another alternative, potentially more useful is to introduce microstructure into the definition of "effective stress". The idea is to look for an alternative definition to the "Bishop-like" effective stress which incorporates a microstructural description of the soil (The formulation of the constitutive model still requires two independent stress variables that combine total stress and suction).

Recently, a proposal has been made in this sense [4] which included the definition of the saturation degree of the microstructure, S_r^m. As mentioned when effective stresses were discussed in Section 3.1, this parameter quantifies the immobile water within the soil. S_r^m may be determined through an interpretation of the pore size distribution of the soil. High clay proportions will result in high values of S_r^m. A predominantly granular material will have a low value of S_r^m. When $S_r^m = 0$ (a sand) the Bishop expression (for $\chi = S_r$) is recovered.

If the proposal is correct, soils that experience a significant change in microstructural volume when compacted to different states or when experiencing suction and stress paths are "complex" materials and they will not be sufficiently well described by a single set of constitutive parameters even if an advanced definition of effective stress, such as the one defined previously in Eq. (6) is introduced in the constitutive formulation. In particular, when $S_r^m = S_r = 1$ the microstructure is always saturated and Eq. (6) becomes the net stress, used in the original formulation of BBM.

The discussion on microstructure and its consequences in terms of mechanical behavior (only in terms of volume change examined) suggests that material parameters are also controlled by the compaction state. In particular, the shape of the LC curve is a piece of information key to interpret the effect of suction on the mechanical response of the compacted soil. In BBM the shape of the LC curve is given by parameters r and β (r establishes a minimum value of the compressibility coefficient for high values of suction and β controls the rate of increase of stiffness with suction). It is then expected that r and β will depend on the type of soil but also on compaction conditions.

Collapse susceptibility of a soil increases when the LC curve exhibits a rapid increase in yield stress with suction. Therefore, in view of the previous discussion, soils compacted dry of optimum should have an LC displaced towards the right, if compared with soils compacted wet of optimum, at the same dry density. This is shown in Fig. 37, which was built using compressibility and collapse data of compacted Barcelona silty clay.

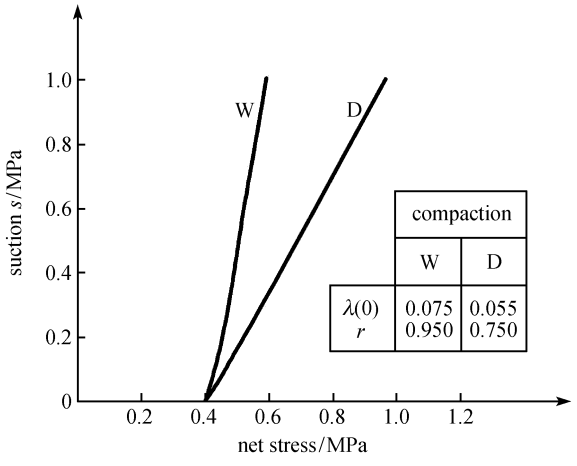

Fig. 37 Yield surface (LC) for samples of compacted silty clay from Barcelona at dry side (D) and wet side (W) to optimum value of water content

The figure may also be interpreted in the sense that compaction dry of optimum leads to a larger elastic domain. Note also that the compressibility coefficient $\lambda(0)$ for saturated conditions is higher for wet of optimum compaction. Modeling this material with BBM implies that specimens located at different points in the (w, γ_d) compaction plane would require different sets of constitutive

parameters. In other words, variations in compaction procedure lead to different soils.

Concepts of soil structure can also be used to explain the different LC curves from Fig. 36. As discussed by Gens et al. [39], the higher preconsolidation stresses in unsaturated conditions found for samples D when compared with samples W are due to the structuring effect of the clayey soil provided by suction. This result is in accordance with that previously mentioned.

The previous discussion has centered on the volumetric behavior of compacted soil. Wheeler et al. [89] also examined the effect of compaction dry or wet of optimum on the critical state lines of compacted kaolin. They found significant differences which led them to conclude that compaction at different water contents essentially produce different materials. More experimental work, involving different soil types, is probably needed to link compaction procedures with material constitutive parameters.

3.2.2 Rockfill

Rockfill offers a significant and reliable strength and it is a favourite solution to stabilize clay cores. Case records of wetting induced settlement have been often reported in the literature for a variety of rockfill dams. El Infiernillo Dam [91], Beliche Dam [92], Ref. [93] and Rivera de Gata Dam [94], Ref. [95] are some examples.

Deformations caused by collapse and long-term effects are typical of unsaturated rockfill and are not treated in general by models for granular materials. This is because grain crushing is not a common observation in laboratory tests on granular materials as it would require very high stress levels to be reached (Ref. [96] among others).

Strength envelopes are nonlinear and depend on suction. Several authors [97–99] showed that the strength envelope was curved, particularly at low stress levels. Nonlinear strength envelopes have been proposed. For instance, De Mello [99] suggested,

$$\tau_f = A(\sigma)^b, \tag{14}$$

where A and b are empirical coefficients. This nonlinearity was attributed to particle breakage during compression and shearing stages. Indices to quantify the amount of particles breakage were proposed by Marsal [97] and Hardin [100]. Large scale triaxial tests [101,102] showing this dependence is more marked in materials prone to particle breakage such as schist and shales. Hard, tough lithologies, with isotropic properties such as limestones exhibit a limited sensitivity to water content changes. Fracture propagation depends also on the size and shape of the fragments.

Flooding rockfill specimens subjected to one-dimensional compression lead to a sudden settlement (collapse) attributed also to the breakage of particles due to rock weakening induced by wetting. Well known experiments were published by several authors [92,97,103]. Wetting tests performed during triaxial testing on large diameter specimens [92,104,105] also identified the partial collapse during the combined effect of mean and deviatoric stress and the reduction of strength of flooded samples if compared with the "dry" ones.

In a recent series of papers the particle breakage mechanism has been investigated in more detail [76–78]. Relative humidity (or, alternatively the total suction) of the "atmosphere" filling the large voids between rockfill particles controls the stiffness of coarse grained materials. Relative humidity, RH, is related to total suction, ψ, by the psychometric law [106]:

$$\psi = -\frac{RT\rho_w}{M_w}\ln(\mathrm{RH}). \tag{15}$$

In Eq. (15), R is the gas constant (8.314 J/(mol·K)), T is the absolute temperature, M_w is the molecular mass of water (18.016 kg/kmol) and ρ_w is the density of pure water (998 kg/m^3 at 293 K). Therefore, relative humidity in the air filling the voids and total suction provide the same information.

Breakage dependence on suction is illustrated in Fig. 38 which shows a set of compression curves, measured in a 30 cm diameter suction controlled oedometer cell, on compacted Pancrudo shale gravel. When fully wetted under stress the saturated compression curve is reached, a behavior also observed in unsaturated soils. Note also that the collapse increases continuously when the confining stress increases. The linear (ε–σ) plot becomes concave towards the σ axis beyond a given strain, which may be identified as 6% in this case. This is an indication of a change in the mechanism of structural rearrangements in the soil specimen.

Figure 39 is a photograph of a particle from a specimen of hard crushed sandstone gravel after being tested in 30 cm diameter oedometer cell with RH control. The specimen was prepared with uniform in size gravel particles ranged between 20 mm and 30 mm. The specimen was not compacted initially and was subjected to a cycle of loading up to 2.3 MPa and then unloading. Breakage found was either concentrated at the grain to grain contacts or it divided the gravel into pieces of significant size. Quite often the failure plane crosses diametrically the initial grain. In other cases, as the one shown in Fig. 39, a more complex fracture pattern is found.

Granular assemblies have been intensely analyzed by means of the distinct element method since the initial work of Cundall et al. [107]. They found that the externally applied stress to a grain assembly is distributed among a number of heavily loaded chains of particles. The particles in those chains receive concentrated loads at some contacts. The remaining particles within the mass are only slightly loaded and they contribute to stabilize the main loading chains. It is therefore reasonable to start the

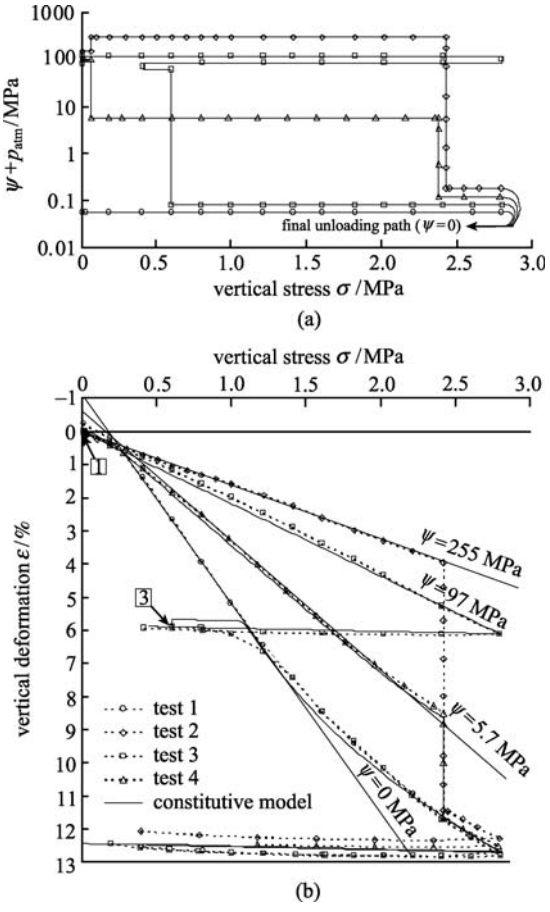

Fig. 38 Oedometer tests on Pancrudo slate. (a) Stress-suction paths; (b) compression curves. Square-enclosed numbers indicate the point of flooding [76]

Fig. 39 Broken particle after test

discussion on particle breakage by considering a single particle, diametrically loaded. The observed grain fracturing in tests suggests that particles break because of the propagation of cracks. In fact, the classical Griffith theory to explain the observed strength of rock specimens relies on a fracture mechanics concept, which attaches a fundamental role to the size of an initial defect or discontinuity.

Assuming a particle idealized as a dish of diameter D and width B, a small flaw is idealized as a central crack of size $2a_i$ aligned with the two opposite concentrated forces. The particle loading is similar to the arrangement of a classical Brazilian test. A uniform tensile stress, normal to the crack, acts on the vertical plane.

A "mode I" type of crack propagation will control the evolution of crack length. Crack propagation in linear elastic mechanics is associated with the concepts of material toughness and stress intensity factor. The latter is defined as

$$K_i = \beta_i \sigma_i^* \sqrt{\pi a_i}, \tag{16}$$

where a_i is the half length of crack, β_i is a non-dimensional factor that depends on (a_i/D), σ_i^* is the stress that would act across the plane of the crack if the particle is not cracked. The stress σ_i^* is related to the overall stress acting on a "specimen" of granular material. Therefore, σ_i^* increases with the applied stress to the granular medium. When K_i, (i stands for a given crack) approaches a material constant, K_c (Mpa·m$^{1/2}$), known as toughness, the crack i propagates at a certain (small) velocity for values $K_i < K_c$. This is the so-called subcritical crack propagation. Cracking depends on the stress intensity factor since the bonds at the crack tip are strained and that makes them more vulnerable to corrosive attack of water. For this reason cracking can occur for stress intensity values smaller than the fracture toughness, justifying the name subcritical given to crack growth under these circumstances.

Crack growth rates reported in several experiments in several materials are collected in terms of (K/K_c) in Fig. 40. The experimental data may be approximated by a simple exponential relationship:

$$V = V_0 (K/K_c)^n, \tag{17}$$

which is a dimensionless version of the Charles proposal [107]. V_0 and n are model parameters. Note that a velocity $V_0 = 0.1$ m·s^{-1} is suggested in Fig. 40 for $K = K_c$.

The exponent n changes with the prevailing suction. Data on synthetic quartz and glass suggest that n increases fast when RH reduces to low values. In other words, under conditions of extreme dryness, crack propagation velocity tends to an extremely low value.

Oldecop et al. [77], based on the expressions for the crack propagation velocity V_i, derived the time for breakage of the particle. They were able to show what is to be expected from a wetting episode (increasing RH): a very significant reduction (several orders of magnitude) in the breakage time. Breakage times in the order of years may reduce to a few seconds. This is equivalent in practice

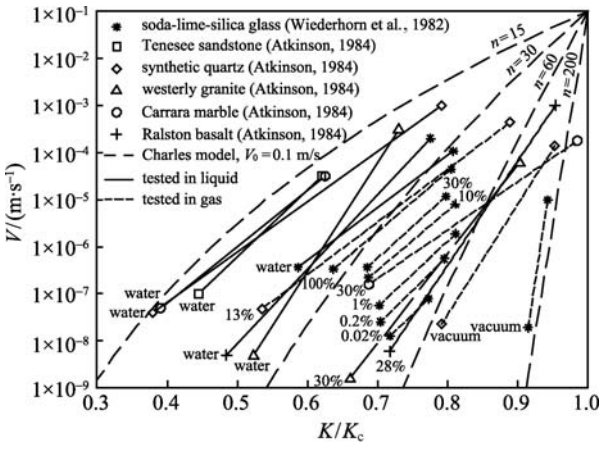

Fig. 40 Crack propagation rates for different rocks, quartz and glass. The testing condition (immersed in water, imposed RH or vacuum) is shown next to each curve [77].

to a sudden breakage and, if the entire granular body is considered, to a sudden deformation (typically a volumetric compression or collapse).

The relationship between crack propagation velocity, stress intensity factor and relative humidity is presented in Fig. 41 [76]. According to Fig. 40 and as shown by experimental evidence, for the same stress intensity factor, velocity increases for increasing relative humidity.

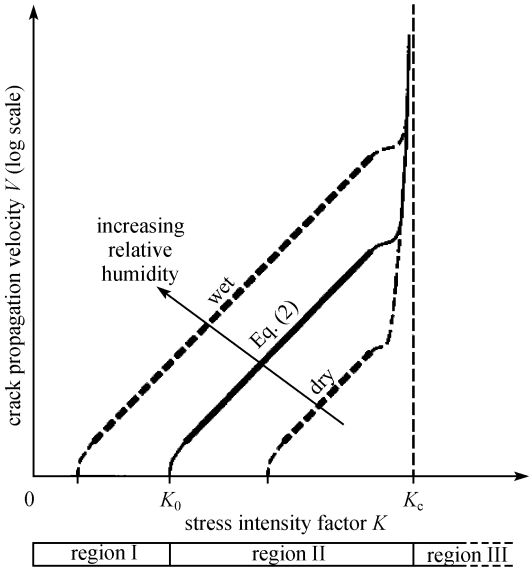

Fig. 41 Crack propagation velocity as function of relative humidity and stress level [76]

With the location in the figure of each crack, it is possible to analyze if it will grow or remain stable. Three regions are defined depending on the stress intensity factor of the crack tip: 1) the cracks in region I will not grow since the stress intensity factor is smaller than K_0 (the fracture toughness defined for that RH and stress level); 2) the cracks in region II will grow with velocity controlled by stress level and relative humidity; 3) the cracks in region III will break instantaneously since the stress intensity factor is higher than the fracture toughness K_c.

Fragments breakage and rearrangement is what explains the time-dependent behavior of rockfill because time is necessary for the relative displacements of the fragments to occur, besides being necessary to establish equilibrium of the relative humidity of the air of the macrovoids and in the crack tips [77,96,97]. Under constant stress (macroscopic stress), fragment breakage and their rearrangement implies changes in the stress distribution of the particles. For this reason cracks can change their place in the plot of Fig. 41 and those that were inactive (in region I) can became active (in regions II and III) and vice versa. Breakage will continue until a stable configuration of the particles is reached. This process also takes time to occur. It can be concluded that the crack propagation mechanism is responsible for primary and secondary deformations of the material since both are associated with deformations due to relative displacements of the fragments, the first due to accommodation and eventually breakage caused by stress changes and the second due to breakage, new rearrangements and stress redistribution.

For a given rock type (characterized by K_c and to a certain extent by a_{0i}) and size of the particle, the breakage time is also very sensitive to the value of the applied stress [77]. Therefore, an increase in σ will result in the immediate rupture of some of the grains and therefore in an immediate deformation even if the initial granular structure is kinematically "locked". The final point is that stressed fissures are always increasing in size, even if the rate is very low. It implies, at the scale of a rockfill, that creep is always present.

Since RH plays such a significant role in particle breakage the next natural step is to perform experiments with suction control (total suction and RH are related through the psychrometric relationship).

Oldecop et al. [76,77] have reported the results of large diameter (30 m) odometer tests in a specially built cell described in Ref. [76]. The tested material was a uniform Pancrudo slate gravel compacted at Normal Proctor energy. The strain time records during each load increment in the tests for two values of RH (50% and 100%) and varying vertical applied stress are consistent with the deformation framework offered by the propagation of cracks in particles. Every load increment leads to an acceleration of the deformation phenomena. After a few minutes the strain log-time curves exhibit steady state creep behavior. The slope of these curves is named secondary compression index and is given by Eq. (18). It increases with applied stress (and eventually becomes constant).

$$\lambda^t = \frac{\mathrm{d}\varepsilon}{\mathrm{d}(\ln t)}. \tag{18}$$

Reducing the suction (wetting) leads also to an increased creep rate. This is shown in Fig. 42. It plots the secondary compression index measured in each load increment in the tests performed under different constant suctions.

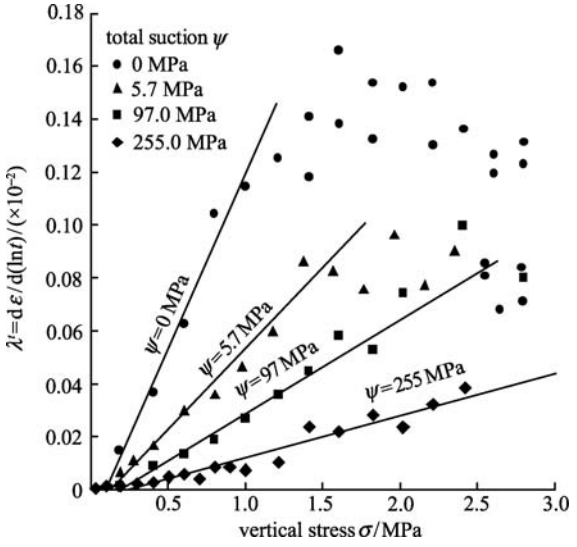

Fig. 42 Effect of applied stress and suction on time dependent compresibility index of Pancrudo slate [79]

For a limited range of stress (0–15 MPa) the data in Fig. 42 shows that the creep coefficient may be described by Eq. (19). This relationship shows the dependence of λ^t on confining stress and suction s. p_{atm} is the atmospheric pressure (p_{atm}= 0.1 MPa) and (μ,β) are model parameters.

$$\lambda^t = \mu p\left(1-\beta\ln\frac{s+p_{atm}}{p_{atm}}\right). \tag{19}$$

Oldecop et al. [76] proposed an elastoplastic model that was consistent with observations and with the underlying fracture propagation framework. In spite of the concavity described when the compression curves previously presented in Fig. 38 were analyzed, it can be observed that they are similar to the compression behavior of a "regular" unsaturated soil since compressibility decreases with increasing suction. In spite of the similarities in the behavior of an unsaturated soil and a rockfill, also significant differences can be pointed out [108]. One of the most important is the existence, in the case of rockfill, of stress and suction states in which water content (or suction) changes do not induce any straining. Another significant feature of compacted rockfill is the apparent lack of elastic domain after compaction.

It is possible to find a constant relation (see Eq. (20) [77]) between the secondary compressibility index λ^t and the compressibility index λ, for which n is a constant that depends on the nature of the material and on the relative humidity/suction. As shown in Ref. [77] the creeping rate does not depend neither on the size of the fragments nor on the applied stress. A similar result had been found by Mesri et al. [109] in the analysis of several results from compression tests on different particulate materials, and also by McDowel [110] based on the simulation of crushing of soil grains using fractal approach.

$$\frac{\lambda^t}{\lambda} \cong \frac{1}{n}. \tag{20}$$

The nature of the materials usually used for rockfill of non-evolutive materials remains practically unchanged after the breakage process since the new smaller fragments maintain the rock characteristics (structure, toughness, etc). However, the global mechanical behavior of the aggregate of fragments (compressibility, strength and dilatant behavior, for example) is affected, mostly because of the changes in void ratio due to the new structural rearrangement of the fragments and their new dimensions and shapes after breakage.

The plastic deformations measured on rockfill samples under oedometeric loading are due to fragments breakage and rearrangement and depend on stress level and on relative humidity. They are time-dependent with constant rate (creeping rate) measured in a relatively short period of time after the stress increment. Therefore, the deformations can be divided into two parts, associated with different mechanisms: immediate deformation mechanism (IDM), and time-dependent deformation mechanism (TDM). TDMs occur while breakage and rearrangement of the fragments are in progress to reach a stable configuration.

Besides suction, breakage depends also on stress. Clastic yielding stress, σ_{ch}, is defined as the threshold value above which fragments will break. Three stages for increasing stress levels [76] can be defined: 1) for low stress levels, stress is smaller than yielding stress ($\sigma < \sigma_y$) and there is only accommodation of the fragments (elastic deformation); 2) for increasing stress levels but with stress smaller than clastic yielding stress ($\sigma_y \leqslant \sigma < \sigma_{ch}$), irreversible deformations occur due to particle rearrangement (plastic yielding, virgin compression); 3) for very high stress levels, when stress is higher than clastic yielding stress ($\sigma \geqslant \sigma_{ch}$) more breakage and crushing occur, with more readjustment (the slope of the virgin compression line changes to account with increasing stiffness due to increasing density).

The strains associated to each stage, $d\varepsilon$, are calculated with Eq. (21), where κ is the elastic compressibility, ψ is suction, λ^i is the slope of the normal compression line when IDM are active and $(\lambda^i + \lambda^d)$ is the slope of the curve when both mechanisms, IDM and TDM, are active. The deformations for each mechanisms are respectively $d\varepsilon^i$ and $d\varepsilon^i + d\varepsilon^d$.

$$\begin{aligned} &\sigma < \sigma_y, && d\varepsilon = \kappa d\sigma, \\ &\sigma_y \leqslant \sigma < \sigma_{ch}, && d\varepsilon = d\varepsilon^i = \lambda^i d\sigma, \\ &\sigma \geqslant \sigma_{ch}, && d\varepsilon = d\varepsilon^i + d\varepsilon^d = [\lambda^i + \lambda^d(\psi)]d\sigma. \end{aligned} \tag{21}$$

The compressibility increment due to long term effects is therefore λ^{d} (see Eq. (22)). This value is always positive and depends on the suction installed since water presence affects fragments breakage, in accordance to the stress corrosion theory previously presented. In Eq. (22), λ_0^{d} is the maximum compressibility index when the material is saturated, p_{atm} is the atmospheric pressure and a_ψ is a constant defined by fitting experimental data.

$$\lambda^{d}(\psi) = \lambda_0^{d} - a_\psi \ln\left(\frac{\psi + p_{atm}}{p_{atm}}\right) \geqslant 0. \quad (22)$$

Collapse deformations are calculated with Eq. (23), where κ_ψ is the compressibility of the material under suction changes, calibrated with experimental data.

$$d\varepsilon_\psi = \kappa_\psi \frac{\psi + p_{atm}}{p_{atm}}. \quad (23)$$

The model proposed by the authors is an elastoplastic hardening model in some respects similar to BBM [38]. Suction has no direct mechanical effect and it is only considered in the compressibility of the material used in the definition of the hardening rule. Another difference is that yield stress for the very dry state is chosen as hardening parameter instead of the yield stress for the fully saturated state.

Chavez developed a large diameter, RH control triaxial apparatus [110] and conducted a program of tests on Pancrudo slate. In this way the previous information, based in one-dimensional compression tests, was completed. Data are presented elsewhere.

The shape of the yield surface (for a saturated material) was determined by an "unloading-probing" procedure described in Ref. [111]. A distinct "cap" was found. Its shape and the plastics strain increments vectors suggests that rockfill hardening is due to volumetric as well as to deviatoric plastic components. The material is not associated, especially in the dilatant regime in the vicinity of the deviatoric limiting conditions.

Chávez et al. developed an elastoplastic model for rockfill [78] which was largely based on the previous compressibility developments to describe the isotropic behavior. The model was based on a number of experimental observations:

1) Critical state conditions were accepted at the end of tests. Suction contributes to maintaining higher void ratios and stress ratios for a given confining stress.

2) Limiting deviatoric states, also controlled by suction, were nonlinear.

3) Two yield loci were proposed: a "deviatoric", where (q/p = constant) and an "isotropic" or "cap". Both are shown in Fig. 43.

4) The deviatoric behavior was described by a hyperbolic hardening rule that is able to model softening. Hardening was described by an effective plastic work and a plastic deviatoric strain. The effective plastic work was a procedure to take into account the rockfill degradation due to particle breakage.

5) The plastic potential was based on a modified Rowe's dilatancy rule.

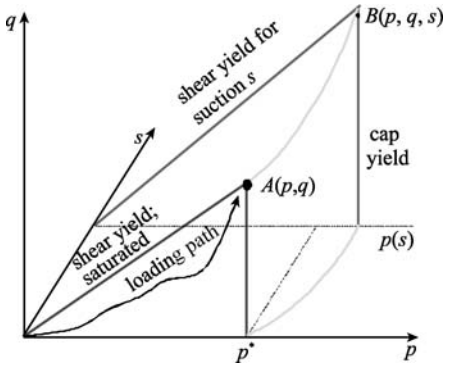

Fig. 43 Elastoplastic model for rockfill [78]

3.2.3 Compacted soft rocks

The hydro-mechanical behavior of compacted marls from Abadia formation in Portugal (upper Jurassic in age) was investigated. The marls were used in the construction of some embankments from A10 Motorway in Portugal (Arruda dos Vinhos). The behavior of the AT1 embankment is reported in Ref. [112]. Some characteristics of the material can be found in Ref. [113]. The evolution in time of the vertical displacements of this embankment was measured during construction and in the following three years. This evolution was compared with settlements measured in different rockfill embankments from dams reported in the literature. The description of the dams and the rockfill materials used in their construction is presented in Table 2. Figure 44 shows the evolution of the displacements in all cases [77].

Figure 44 shows that the vertical displacements increase for a long time after construction. The highest rates occur in the first year after construction. The deformations observed can be explained by the breakage of rock fragments due to filling the dam reservoir, in the first year, followed by the rearrangement of the rockfill structure.

Because of the compaction conditions adopted in the construction of A10, the main part of the degradation occurred during the construction. Similar conditions may not be achieved in other cases.

Because of the height of dams, their stresses are much higher than in the embankments of A10. High stresses plus, in certain cases, the percolation, are favourable to rockfill crack propagation [76,77], justifying the delayed deformations observed in the dams. Moreover, the construction method and the toughness of the rockfill material control also the cracking rate. In the first case,

Table 2 Dams presented in Fig. 44 [112]

dam	description	height/m	type of rock
Chocón	central core, gravel shales	90	shales
Alicurá	central core, gravel shales	130	shales
Murchison	CFRD/ compacted rockfill	94	volcanic rocks, quartzite
Cethana	CFRD/ compacted rockfill	110	quartzite, quarried
Alto Anchicaya	CFRD/ compacted rockfill	140	metamorphic sediments, schist and chert
Foz do Areia	CFRD/ compacted rockfill	160	basalts and basaltic breccia
Mackintosh	CFRD/ compacted rockfill	75	greywackle, slate and philite, basaltic-andesitic rocks
Exchequer	CFRD/ dumped rockfill	150	volcanic rocks, quartzite
El Infiernillo	central core, rockfill shells	146	diorite
Dix River	CFRD/ dumped rockfill	84	limestone and shale
Nanthala	CFRD/ dumped rockfill	80	limestone and shale
Beliche	central core, rockfill shells	64	fractured schists in the inner shells and greywacke in the outer shells
Rivera de Gata	central core, rockfill shells	50	metamorphic granites, quartzites

Note: CFRD is concrete faced rockfill dam.

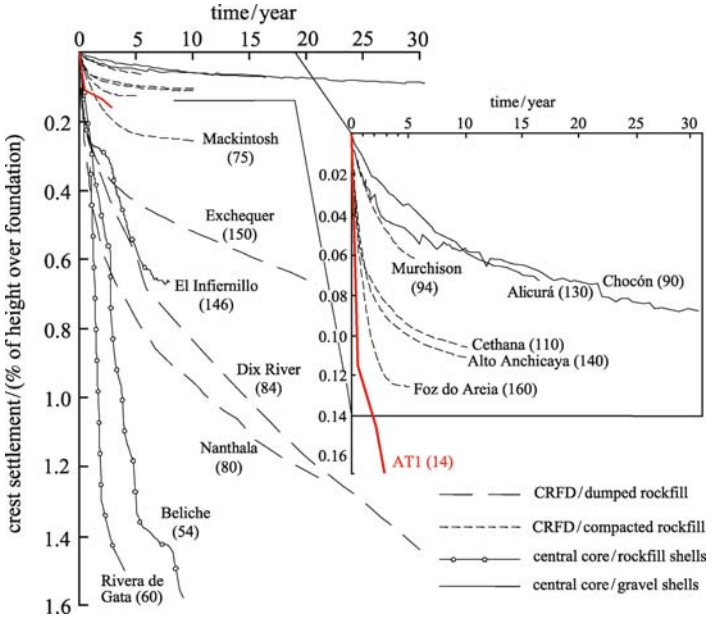

Fig. 44 Long term deformations measured in several dams after their construction [77]

larger settlements are expected for dumped rockfill than for compacted rockfill due to the initial void ratio. This is confirmed by the results presented in Fig. 44. In the second case, the dams built with lower quality rockfill (see Table 2) are those that show higher displacements rate. The creeping deformations can be related with the deformations in Fig. 44 as soon as they show some stabilization.

In spite of the differences between the rockfill dams referred and AT1 embankment, their long term behavior can be compared. The deformations measured in AT1 in the last two years, also in Fig. 44, show a decreasing annual speed [112]. The rate of the deformations of AT1 is very similar to those found for Rivera de Gata Dam in the first years. This indicates that their long term trends are similar. The deformations for all cases can have the same nature. It can be interpreted that AT1 deformations are due to the rearrangements of the fragments.

Considering that the stresses installed in the embankment are lower than in the dams presented and that there is no percolation, it can be assumed that creep deformations of the embankment built with fragments of soft rocks occur at strain rates higher than in dams built with rockfill (fragments of non-evolutive rocks). Probably this is due to the evolutive nature of soft rocks used (marls). They are

more prone to crack than harder rocks because they generally have inferior strength and stiffness and their structure can be strongly affected by loading and suction cycles. For a correct evolution of the deformations of AT1 during its lifetime it is therefore necessary to consider long term effects. This conclusion can be considered to be valid for embankments built with soft rocks in general. The expected long term deformations in AT1 will be the result of viscoplastic phenomena associated with particle rearrangement and also to the degradation of marls due to wetting and drying cycles imposed by atmospheric actions.

Consider now some experimental information. Figure 45 presents the vertical deformations measured during the full saturation under low vertical stress of two samples of compacted marl. The test was performed to show the effect of the degradation of the fragments in the deformation of the compacted material. The behavior of one uniform grading-size sample prepared with initial void ratio equal to 1.078 was compared with the deformation of a sample prepared in a similar manner (same energy and water content) but with the voids between the fragments filled with a fine fraction of the same soil (initial void ratio equal to 0.637).

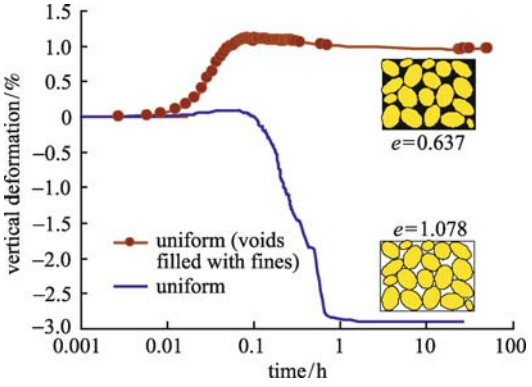

Fig. 45 Comparison between oedometer tests performed in uniform grading size samples with and without the voids being filled with a fine fraction (full saturation under vertical stress = 9 kPa)

The swelling observed for the sample with the voids filled, compared with the large global collapse exhibited by the sample with the larger voids confirms the degradation of the fragments invading the large pores between them. At the limit, when the degradation process is completed for all the fragments, a soil will be obtained (reconstituted material). Therefore, the compacted marls experience a transition between a rockfill-like behavior (when the fragments are intact) and the behavior of a clayey material (when the degradation accumulates).

The degradation of the fragments increases with vertical stress and with the combined effect of stress and suction changes. The photographs shown in Fig. 46 are from two specimens of compacted marls after being loaded in oedometric conditions to a 1000 kPa vertical stress. The first specimen was loaded dry (compaction water content) and the second was loaded in fully saturated conditions. The fragments in the second specimen can hardly be distinguished. The degradation of the fragments caused by the combined effect of stress and suction changes was also measured in several other tests described in Refs. [112,113]. Wetting and drying cycles simulating the effects of atmospheric actions were applied because suction cycles are one of the main causes of degradation of the fragments of marl.

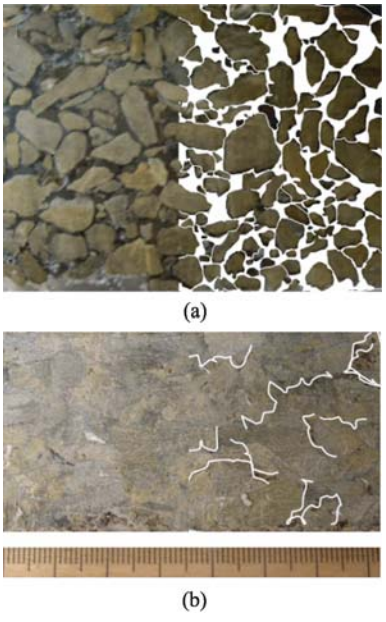

Fig. 46 Macrostructure of the compacted sample under different suction cycles for vertical stress of 1000 kPa. (a) Dry to $s = 230$ MPa ($e = 0.978$); (b) fully saturated ($e = 0.505$)

It is assumed that compacted marls behave like an assembly of fragments to which is added the effect of their degradation, as illustrated in Fig. 47. In this case, global irreversible volumetric deformations Δe^{p} (see Eq. (24)) are the sum of the irreversible volumetric deformations of the fragments $\Delta e^{\mathrm{p}}_{\mathrm{b}}$ (debonding or structure lost) and of the irreversible volumetric deformations of the macrostructural rearrangement $\Delta e^{\mathrm{p}}_{\mathrm{M}}$. The new term $\Delta e^{\mathrm{p}}_{\mathrm{b}}$ can be seen as the contribution of the plastic deformations of the microstructure $\Delta e^{\mathrm{p}}_{\mathrm{m}}$ to the plastic deformations of the macrostructure. These deformations are not easily quantified:

$$\Delta e^{\mathrm{p}} = \Delta e^{\mathrm{p}}_{\mathrm{M}} + \Delta e^{\mathrm{p}}_{\mathrm{b}}. \tag{24}$$

Figure 48 presents the main results of the oedometer tests performed. The compressibility index in the elastoplastic range decreases with increasing suction, a result expected for unsaturated compacted materials ($C_{\mathrm{c}} = 0.535$ for $s = 2$ MPa, 0.422 for $s_1 = 38$ MPa and 0.379 for $s_2 =$

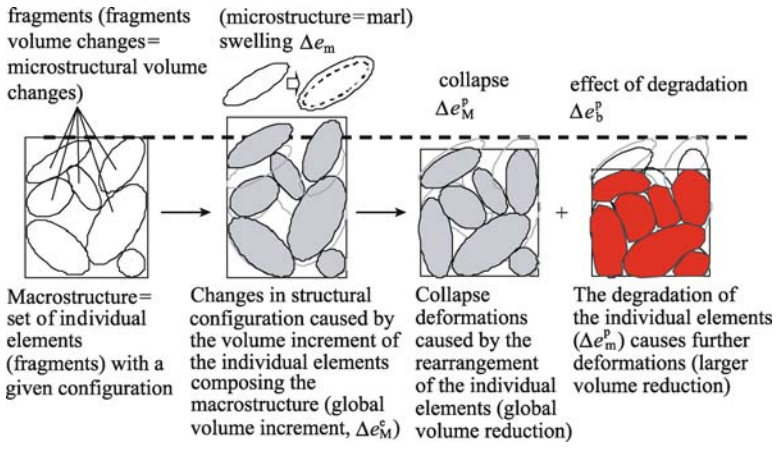

Fig. 47 Effect on global behavior of fragments degradation due to full saturation [112]

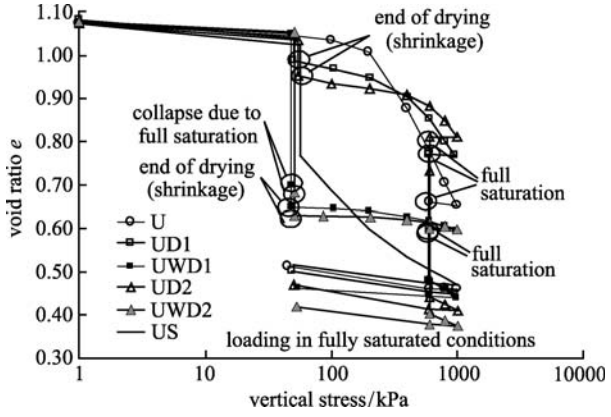

Fig. 48 Oedometric tests [112]

230 MPa for tests U, UD1 and UD2, respectively). The elastic compressibility is very similar for the two UD tests (average value C_s= 0.006). A value of C_s= 0.035 was measured in the U test. This result indicates that drying has some effect in the structure of the compacted material.

The effect in the mechanical behavior of wetting before drying (tests UWD) is studied by means of the comparison between tests UD and UWD for the suctions 38 MPa and 230 MPa. Note that wetting at σ_v= 50 kPa in tests UWD led to a strong collapse and therefore to a reduced void ratio. Subsequent drying did not modify the void ratio. The denser UWD specimens are therefore expected to be stiffer than samples UD. This is shown if C_c values are compared (C_c= 0.422 and 0.379 for specimens UD1 and UD2, and 0.107 and 0.070 for specimens UWD1 and UWD2). Small differences were found in the elastic compressibility independently from the past suction history.

Under 600 kPa, a larger collapse was observed for the samples UD than for samples UWD, a result expected due to the different void ratios of the samples before full saturation. The compressibility curves for all samples loaded under fully saturated conditions (see Fig. 48) are very similar, indicating a similar structure. The final void ratio found for the saturated samples shows some differences, however, indicating different structures. This result is explained possibly by the double structure of the compacted material.

Irrespective of the degradation of the fragments when fully saturated, the compacted material, when dry, behaves as a rockfill. In fact, for the unsaturated samples a marked time-dependent behavior was observed under each loading increment in oedometer tests performed under constant suction. Increasing slopes of the curves in a plot deformation $d\varepsilon_v$ vs ln$t$ were measured. This is expected in rockfill materials, previously described. The secondary compression index λ^t given by Eq. (18) measured in each test is presented in Fig. 49(a). This figure is identical to Fig. 42 previously presented. The values measured for the vertical stress σ_v= 1000 kPa are in Fig. 49(b). The value found for the saturated test is included in the figure.

The peak reached before full saturation shown in Fig. 49 (b) marks the transition between rockfill behavior (above a given suction) and clayey soil behavior (below that suction). The threshold suction identified is the minimum suction studied (2 MPa). However further study is required to investigate this value.

Figure 49(b) also includes the values of λ^t measured in the unsaturated oedometer tests performed in compacted rockfill presented previously in Fig. 42. They show that the peak is found at full saturation when the breakage is more intense. The comparison confirms that compacted marls experience a qualitative change in behavior when wetted. Particle breakage dominates at high suctions. Regular soil deformation is found at lower suctions.

The two aspects of behavior described for compacted marls are covered by constitutive models for rockfill and for regular compacted soils, respectively. Therefore it can be concluded that the mechanical behavior of this material is a complex combination of the mechanical behavior of

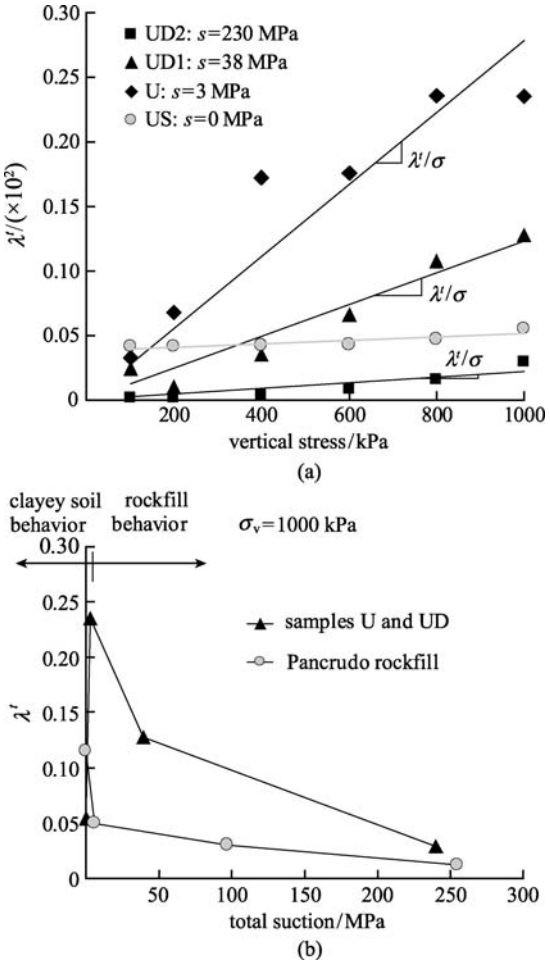

Fig. 49 Values of λ^t for samples UD and full saturated US. (a) Changes with increasing vertical stress; (b) transition between rockfill and clayey soil behavior [112]

the two soil types presented previously as boundary cases of behavior (rockfill and regular compacted soils). Eventually this conclusion is valid for all mixtures of materials.

However, the definition of the model to be adopted for a complex material is not simple. It is probably wise to base it in the two models presented in the previous sections but requires additional new features. The resulting model must be able to simulate the deformations due to the degradation of the fragments under loading paths involving stress and suction changes because this is what makes the material different from the two boundary materials.

The characterization tests performed by Cardoso [112] on compacted samples of marl included the quantification of structural changes caused by different loading paths. The results of MIP tests (micropores) were joined to data from the measurement of the macropores dimensions to cover the large range of dimensions of the voids of the compacted material. The process used in the measurement of the macopores is described in Ref. [112]. The results found for the compacted material at the compaction water content (U), after being fully saturated (US) are in Fig. 50. The samples loaded to 1000 kPa vertical stress in the figure (samples identified with −1000 kPa) are the samples previously presented in Fig. 46.

Figure 50 shows a predominant size in the low diameters attributed to the voids of the microstructure (microvoids) and several peaks in the large diameters (see Fig. 50(b)) attributed to the macropores. The microvoids are those of the rock because similar MIP plots were obtained in rock samples. The macropores concern the large voids between the fragments. As espected, their sizes exhibit large changes after stress and suction changes. However the micropores also change essentially with suction changes. Therefore the material classifies as a material where the contribution of the microstructure for global behavior is very important.

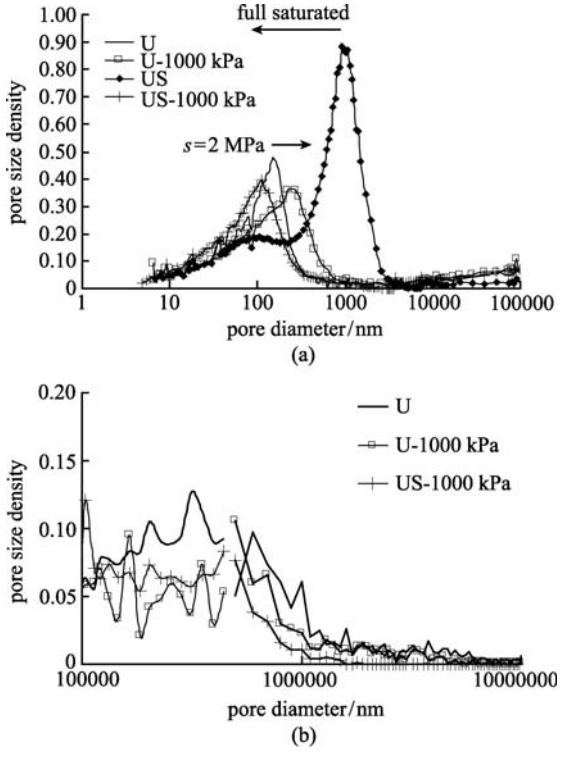

Fig. 50 Pore size distribution of compacted material under different loading paths. (a) MIP and measurement of macropores; (b) zoom for large diameters [112]

The information from the pore size distribution of the compacted material allows identifying three structural levels: the macrostructure is the arrangement of fragments, the mesostructure is the fragment and the microstructure is the microstructure of the rock (mainly clay minerals). For simplification only two structural levels are considered.

From a general point of view, traditional unsaturated constitutive models are not adequate to reproduce the large

amplitude of the deformations observed in the compacted marls caused by their degradation on wetting. On the other hand, models for hard rockfill materials are not adequate because they are not able to reproduce the behavior of the material after the strong degradation of the fragments. These two reasons, added to the finding of the double structure detected in the material, lead to the conclusion that a model for regular compacted soils is probably adequate. For this reason, BExM proposed by Ref. [39] for expansive clays is the model used as starting point to reproduce the behavior of the compacted marls.

According to BExM, the mechanical behavior of each structural level will be simulated with adequate constitutive models. BBM is used for the macrostructure. For the microstucture, the fragments, two alternatives can be adopted. In the first proposal an elastic constitutive model can be used, such as the model included in original BExM. In the second, a more complex but more realistic constitutive model for the fragment can be used. Since the material of fragments is an evolving rock, a model for structured materials was used. It was chosen the model proposed by Alonso et al. [114] for soft rocks. This model is itself a double structure model with the particularity of including a debonding parameter b at the level of the microstructure that is also responsible for macrostructural changes. This is the only model known, so far, that considers two structural levels in the formulation and also includes debonding.

Marls are treated as cemented materials, common in nature. Alluvial and colluvial soils wind-blown deposits, tropical soils and a wide variety of soft clayey rocks or hard soils are other examples of cemented materials. The stiffness and strength of these materials are affected by wetting and drying cycles. Loading and unloading is also capable of inducing "damage", a term which makes reference to the integrity of the initial cementation. Soft rocks, because of the usual expansivity of the clay matrix, are especially sensitive to suction changes. Debonding in this case is explained to be caused by the expansion of clay minerals in a bonded matrix. It is as if the clay stacks would act as micro flat jacks inducing damage in the bonds. Figure 51 presents a scheme of cemented materials where clay aggregates made of clay minerals are connected with physical connections, the bonds.

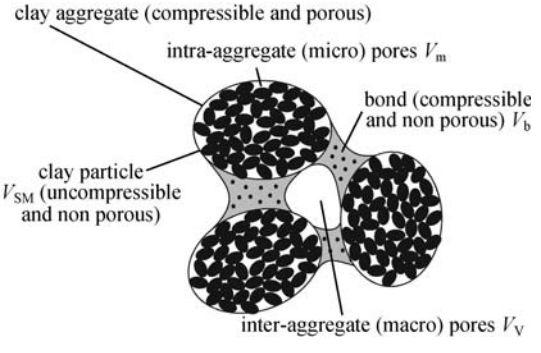

Fig. 51 Structure of a bonded material [115]

For the microstructure, bonding affects the elastic compressibility of the material given by the elastic compressibility index $\kappa_m(b)$ (see Eq. (25)). A linear variation of $\kappa_m(b)$ with b is proposed, where κ_{mfd} is the microstructural compressibility for the fully debonded material. It was measured in experimental tests performed in specimens of reconstituted material prepared as indicated by Burland [116].

$$\kappa_m(b) = \kappa_{mfd}\left(1 - \frac{b}{b_0}\right). \tag{25}$$

The microstructural void ratio e_m is given by Eq. (26) where e_{m0} is its initial value and p' is the effective stress at this structural level.

$$\begin{aligned} e_m &= e_{m0} - \kappa_m(b)\ln\frac{p'}{p'_{max}}, \text{ if } p' \leqslant p'_{max}, \\ e_m &= e_{m0}, \text{ if } p' > p'_{max}. \end{aligned} \tag{26}$$

In Eq. (26) a limiting value of the maximum vertical stress acting in the microstructure p'_{max} is introduced to consider the physical fact that no deformations can occur for high confining stress irrespective of the current bonding. Bonding controls the development of microstructural strains below p'_{max}. In the simulation it is assumed that the stress level acting in the microstructure is always below p'_{max}.

The damage parameter b was proposed [112] to depend on suction s besides accumulated plastic strains $\delta\varepsilon_v^p$ ($b = 0$, fully debonded material; $b = b_0$ initial bonded material). This parameter is given by Eq. (27) proposed by Alonso et al. [117], where b_0, Δb, a and h_1 are constants calibrated to fit experimental data. The effective stresses for the microstructure were defined using Eq. (6) previously presented, where $\alpha = 4.56$ (calibrated with swelling tests performed) and the saturation degree was defined using van Genuchten [118] expression calibrated also with experimental data [112]. The validation of the model was performed in the simulation of oedometer tests performed on rock samples under different stress and suction paths [112].

$$b = [b_0 - \Delta b(1 - e^{-as})]e^{-h_1\int|\delta\varepsilon_v^p|}. \tag{27}$$

BBM parameters for the macrostructure were defined through experimental data. The parameters are presented in Table 3. The constants f_0, f_1 and n of the interaction functions, given by Eq. (28), were calibrated numerically.

$$f(p) = f_0 + f_1\left(1 - \frac{p}{p_0}\right)^n. \tag{28}$$

Oedometric tests on compacted specimens were conceived to find BBM parameters for the macrostructure also

Table 3 Model parameters [112]

fragment (microstructure of compacted material)			
macro	micro (see Eq. (25))	interaction function	
$\lambda_{M(0)} = 0.027$	$\kappa_{mfd} = 0.030$	wetting	drying
$r = 0.65$	parameter b (see Eq. (27))	$f_0 = -7$	$f_0 = 0.8$
$\beta = 0.05\ \text{MPa}^{-1}$	$b_0 = 0.9$	$f_1 = 7$	$f_1 = 0$
$\kappa_M = 0$	$b_i = 0.75$	$n = 1.0$	$n = 1.0$
$\kappa_{sM} = 0$	$h_1 = 2$		
$p_0^* = 858$ kPa	$\Delta b = 0.04$		
$p^c = 280$ kPa	$a = 2.1$		

macrostructural arrangement (macrostructure of compacted material)				
macro	interaction functions (see Eq. (25))			
$\lambda_{M(0)} = 0.25$	before fragments degradation		after fragments degradation	
$r = 0.23$	1st drying	1st wetting	2nd drying	2nd wetting
$\beta = 0.03\ \text{MPa}^{-1}$	$f_0 = 0$	$f_0 = -12$	$f_0 = -0.5$	$f_0 = -5$
$\kappa_M = 0.006$	$f_1 = 0$	$f_1 = 5$	$f_1 = 0$	$f_1 = 7$
$\kappa_{sM} = 0$	$n = 1$	$n = 1$	$n = 1$	$n = 1$
$p_0^* = 80$ kPa				
$p^c = 47$ kPa				

presented in Table 3. They also provided the experimental compressibility curves to be reproduced with the model. The adoption of a single set of parameters for the material before and after being fully saturated is justified because it is the same material. This is equivalent to consider that the material becomes denser after the degradation of the fragments.

The tests were performed in uniform grading size samples prepared with marl fragments with diameters ranging from 9 mm to 4.7 mm. Water content of the fragments ($w = 14\%$) and void ratio ($e = 1.078 \pm 0.05$) was the same for all specimens [112]. Two sets of tests were performed, named UD and UWD. The tests from set UD were performed on samples dry to $s_2 = 230$ MPa following loading paths defined to find BBM parameters. Two of the samples were partial wetted under a 600 kPa vertical stress to suctions $s_1 = 39$ MPa and $s_3 = 12$ MPa (specimens UD2-1 and UD2-3, respectively).

Maximum vertical stress reached in the oedometric loading process under constant suction was 1000 kPa. Then the samples were fully saturated after being unloaded to 600 kPa, and then reloaded to 1000 kPa and unloaded. The tests from set UWD are similar to tests UD but the samples were fully saturated before being dried to $s_2 = 230$ MPa. The loading paths followed are presented in Fig. 52.

Besides the adoption of a constitutive model for structured materials for the microstructure, the presence of the fragments was considered in the definition of the interaction functions. Because the fragments degrade (which explains the strong structural changes suffered by the compacted material) two interaction functions were necessary for each suction path. Details are described in Ref. [112].

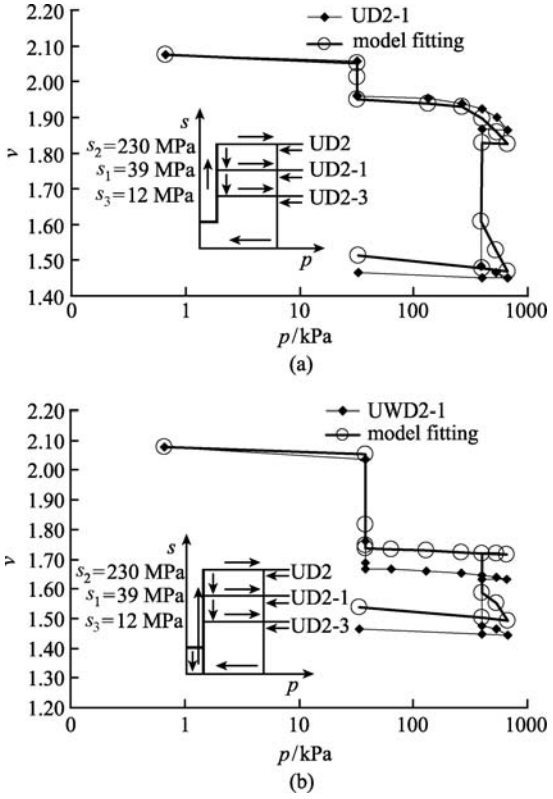

Fig. 52 Stress paths and reproduction of tests on compacted samples [112]

Finally, the comparison between the numerical and experimental curves for the tests is given in Fig. 52 for the samples where the increment of vertical stress was applied under s_1= 39 MPa (specimens UD2-1 and UWD2-1). It can be observed that the main features of the behavior of the compacted material are reproduced: shrinkage occurs on drying, collapse occurs in partial wetting and after full saturation and the numerical and experimental curves are similar under the application of vertical stress in unsaturated conditions.

As final conclusion, the definition of the model for the behavior of the microstructure and of the interaction function between the two structural levels was fundamental to reproduce the tests. This is because the microstructure (the fragment in this case) strongly affects global behavior. Compacted marls therefore are a compacted material classified as complex. This indicates that the definition of an adequate constitutive model for the microstructure is the key factor to be considered. Finally, the model must be defined for triaxial states also. This is the object of future work.

3.3 Main features of the behavior of unsaturated materials used in dams

Figure 53 synthesizes the information gathered considering mainly the sizes of the particles as it was done previously in Fig. 22. It includes the Casagrande classification of soils (GW, GP,..., CL, CH) because it is believed to provide a useful link to design practice. Also included is the main effect of water in soil pores on its mechanical behavior. In this case water is considered through the suction concept, which is included in constitutive models.

In Fig. 53, the following main points must be highlighted:

1) The dimensions of rockfill and gravels varies between centimeters and meters. The deformations result from fragments breakage and changes in the granular structure. Rockfill properties (strength, deformation, long term creep, collapse phenomena) are strongly linked to particle breakage. Particle breakage, in turn, depends on the stress concentrations at particle-to-particle contacts and on the prevailing relative humidity (RH) at each particular contact (which will presumable be in equilibrium at a larger scale). Soil density is important as it provides an idea of the number of contacts and, therefore, of stress concentration points. In a series of publications [76–78] a phenomenological elastoplastic constitutive framework has been described. The resulting model has similarities with elastoplastic models conceived for “regular” unsaturated soils and, in particular, with BBM.

2) Sands are materials with grain size ranging from 10 mm to 0.1 mm. The number of contacts between the grains increases significantly for these materials when compared with rockfill. Therefore the concentrated stresses at the contacts decrease in intensity and the stress intensity factor is much lower than the material toughness, the property that measures the likelihood of grain breakage. Grain breakage is unlikely to occur unless extremely high stresses are applied to these materials and the effect of relative humidity in crack propagation is irrelevant. On the other hand, for the smaller grains of sand the capillary effects become more relevant due to the menisci at the air-

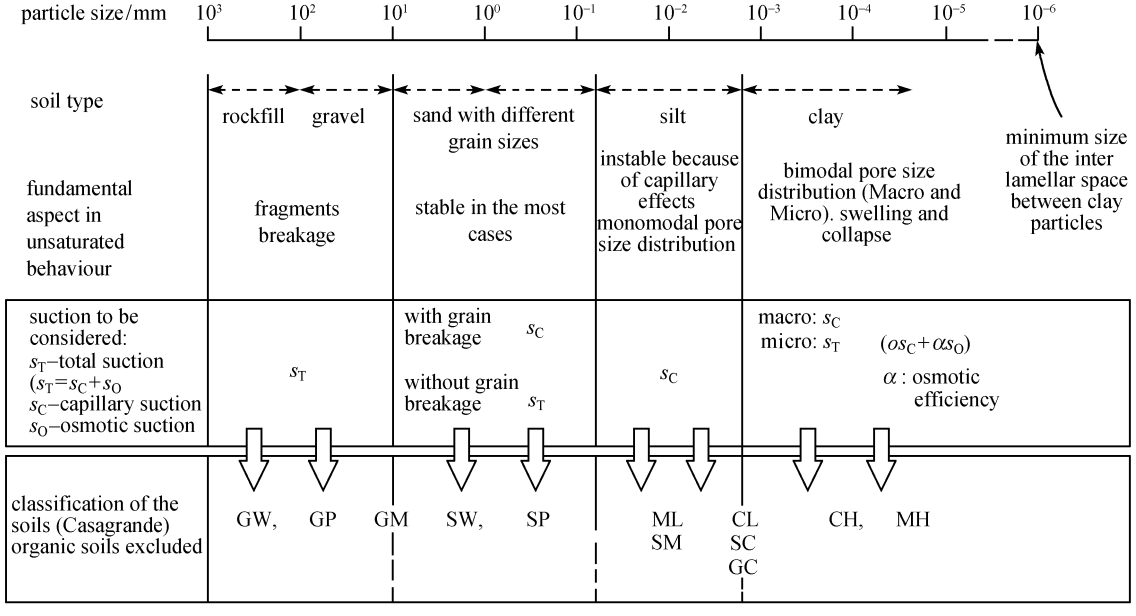

Fig. 53 Synthesis of main aspects to be considered for different soil types proposed in Section 3.1

water interface. These effects may not be very important for mechanical behavior since gravitational forces are still dominant.

3) Silts are non-plastic materials where the dimensions of the grains range from 8×10^{-2} mm to 2×10^{-3} mm. The capillary forces earn relevance because gravitational forces decrease. Capillary suction is therefore very important to explain the behavior of this type of soils and acts increasing soil stiffness and strength. The effect of suction is to pre-stress soil structure. The microstructure is not particularly relevant and a monomodal pore size distribution is expected.

4) The most important changes in the main features of the behavior of the compacted materials occur in the transition between silts and clayey soils. The material shows a bimodal structure where two dominant pore sizes can be identified with distinct orders of magnitude. They are the macro and the micro pores. Capillary effects dominate at the large pores but physico-chemical phenomena explained by the presence of electric charges are also important. It is usual to assume that the clay aggregates remain saturated as explained previously. Osmotic suction is relevant in this case. The two components of suction suggest that total suction must be considered in constitutive models for clays and for all the materials with double porosity in which the microstructure is active (these are "complex" materials). The behavior of these materials is complex because capillary suction controls the deformation of the aggregates as in a granular medium, the macrostructure, and the osmotic pressure, controls in part the deformations of the microstructure or of the aggregate itself.

According to the description in Fig. 53, the relationship between suction and grading size distribution is immediate for the type of soils where the sizes are well distributed. Such is the case of rockfill and uniform grading size granular materials. However, for compacted clayey soils and for the soils previously classified as mixtures, this correspondence is not easy. The mixtures in this case are made of granular materials with an important percentage of fines and both may or not have the same geological origin. In all cases the material has a marked double structure where the microstructure may have an important contribution to global behavior. As a result, these materials have a complex behavior. However, as mentioned in Section 3.2 for regular compacted soils, the materials where the microstructure is not active may be reproduced with simpler constitutive models such as BBM.

The main features of behavior to be reproduced with the

Table 4 Comparison between unsaturated rockfill, unsaturated soil and unsaturated compacted soft rock

	rockfill	compacted soil	compacted soft rock
overall behavior on wetting	collapse associated with fragments breakage and rearrangement	collapse associated with structural changes. It is caused by the hardening mechanism and the interaction between the two structural levels.	collapse associated with fragments breakage, rearrangement and destructuration and also due to swelling of the fragments invading the macropores
important properties of the fragments/ clay aggregates	Particle toughness is a fundamental property.	Particle strength does not affect the overall behavior.	Particle toughness, stiffness and its changes with loading (stress and suction change) are fundamental properties.
water induced effects/ suction influence on global behavior	The effect of suction is to control particle breakage velocity.	The effect of suction is to pre-stress soil structure. It affects the volume changes of the two structural levels.	The effect of suction is to induce damage measured by breakage and strength and stiffness reduction. It must be considered at the level of the fragment and of the aggregate.
suction to be considered	Total suction controls water induced effects	Matric suction controls water induced effects. When relevant, osmotic suction controls microstructural volume changes.	Total suction controls water induced effects in the macrostructure and matric suction controls it inside the rock fragment. When relevant, osmotic suction controls microstructural volume changes.
main cause of structural changes	A threshold toughness to initiate fracture propagation is included in the model through a parameter σ_y. For $\sigma < \sigma_y$ no time delayed deformations exist (no collapse).	Collapse explained by structural instability. The volume changes of the microstructure affect the macrostructure. In double structure models are reproduced by the interaction between the two structural levels.	For high suctions the cause is identical to rockfill. Behind a threshold suction value (near saturation) fragments degradation occurs. This value may be controlled by the air entry value of the fragment.
existence of long term deformations	Long term deformations are caused by fragments breakage and rearrangement. These deformations (including collapse) are inhibited for very dry states.	There is no equivalent concept. Eventually, long term effects are explained by hydrodynamic consolidation in case of full saturation.	For the macrostructure the behavior is similar to rockfill for very dry states. For the microstructure it can be due to water transference between the macrostructure and the microstructure. Long term effects are due to the delayed volume changes of the microstructure caused by its small permeability.
yielding definition/ hardening rule	Yield stress for the very dry state is conveniently chosen as hardening parameter	Yield stress for the saturated soil is chosen as hardening parameter	Yield stress for the aggregate is chosen as hardening parameter. The yield stress of the rock must also be considered in the constitutive model of the microstructure (fragment).

constitutive models for the different types of materials described in Section 3.2 and the information provided in Fig. 53 can be synthesized as shown in Table 4.

One significant feature of compacted rockfill is the apparent lack of elastic domain after compaction. For this reason the model used considers yield stress for the very dry state as hardening parameter and only simulates collapse on wetting. The intensity of collapse depends on the susceptibility of the rockfill particle to break under stress and RH changes. Toughness and strength are important properties of the grains. Long term deformations are explained by particle breakage, with velocity controlled by RH, fragment's size and material properties. Total suction is computed from current RH.

Regular compacted materials are double structure materials where a macrostructure and a microstructure can be identified. They can be classifies as simple materials, when the behavior is controlled by macrostructural behavior, or by complex materials, when global behavior is significantly affected by the existence of a microstructure. Water effects are controlled by total suction since capillary (matric suction) and chemical effects (osmotic suction) are present. The latter are important only for the complex highly expansive materials (important clay fraction and mineralogy of the clays present).

For simple compacted materials, capillary suction acts as a pre-stressing of the the soil. Swelling on wetting and shrinkage on drying are interpreted as elastic behavior. Collapse is associated with irreversible structural changes; therefore saturated yield stress is chosen as hardening parameter. Long term deformations are not important unless they are associated with hydrodynamic consolidation in full saturated cases. In double structure complex materials, they may be explained by the delay on the hydration of clay aggregates caused by the different permeabilities of the two structural levels.

Compacted soft rocks are complex compacted materials where the microstructural volume changes (degradation of the fragments) are fundamental to explain global behavior. However the physical properties of the fragments are important, as they are in rockfill materials, since macrostructural volume changes are caused by fragments breakage and rearrangement in very dry states. However the model used for the microstructure must be analyzed properly. Besides the adoption of adequate rules for bond degradation, the model must incorporate the changes in the mechanical properties of the rock due to its degradation when wetted. Because it is a double structure material and microstructural deformations are so important, special care must be taken in the definition of the interaction function between the two structural levels. An attempt to develop a model for compacted marls is made in this work, based on double structure models because they are more likely to be suited since the macrostructure and the microstructure can be defined with independent mechanical constitutive models.

In a general sense, the model for mixture materials must deal with the two types of behavior. The dominant type must be identified for example by interpretation of MIP, WRC and swelling tests, as it was done for the compacted marls. Then, one of the two types of behavior must be adopted and adapted to reproduce the most important phenomena present. Other constitutive models can be included, such as models for cemented materials, as long as they are compatible with the framework adopted for global behavior.

4 Conclusions

The experience earned in the last few decades allowed the definition of constitutive models able to reproduce the behavior observed in practice. Concepts of unsaturated soil mechanics are fundamental for the understanding and definition of these rules. They also allow identifying the deformation mechanisms caused by water, which are basically interpreted by suction and its two components.

The idea of a unique constitutive model to reproduce the behavior of all types of soil is abandoned. This is because the physical mechanism behind the deformation processes is very different at a fundamental level (particle or pore) for the variety of geomaterials found in nature. Considering the materials traditionally used in the construction of earth and rockfill dams, the behavior of the unsaturated soil types proposed can be reproduced using constitutive models from typical of regular compacted soils or from rockfill. The fundamentals behind the definition of the two distinct constitutive models were presented. They are very distinct and are based, among other factors, on the role of water in the soil and how it is affected by soil structure and mineralogy.

The prediction of the deformations of structures built with non-traditional materials requires the definition of adequate unsaturated constitutive models. This is a current research topic. An attempt to develop a model for compacted marls is made in this work, where a double structure model was adopted to the particular nature of the materials. Such an approach is considered to be valid for other types of materials.

References

1. Olivella S, Gens A, Carrera J, Alonso E E. Numerical formulation for simulator (CODE_BRIGHT) for coupled analysis of saline media. Engineering Computations, 1996, 13(7): 87–112
2. UPC-DLT (2002). CODE_BRIGHT- User's Guide. Departamento deIngeniería del Terreno, E.T.S. Ingenieros de Caminos, Canales y Puertosde Barcelona, Universidad Politécnica de Cataluña, Spain
3. Alonso E E, Pinyol N M. Unsaturated soil mechanics in earth and rockfill dam engineering. In: Toll D G, Augarde C E, Gallipoli D, Wheeler S J, eds. Proceedings of the 1st Europe Conference,

E-UNSAT 2008, Durham, United Kindom. London: Taylor and Francis, 2008, 3–32
4. Alonso E E, Rojas E, Pinyol N M. Unsaturated soil mechanics. In: Proceedings of XXIV Reunión Nacional de Mecánica de Suelos, Mexico. 2008
5. Maranha das Neves E, Cardoso R. Structural behavior of embakments built with unsaturated materials – Application to the embankments from A10 Motorway, Arruda dos Vinhos / Carregado. Study for BRISA. Department of Civil Engineering, Institute for Structures and Construction, Report ICIST EP 13/08, Instituto Superior Técnico, 2008
6. Ng C W W, Pang Y W. Influence of stress state on soilwater characteristic and slope stability. Journal of Geotechnical and Geoenvironmental Engineering, ASCE, 2000, 126(2): 157–166
7. Hoffman C, Tarantino A. Effect of grain size distribution on water retention behavior of well graded coarse material. In: Toll D G, Augarde C E, Gallipoli D, Wheeler S J, eds. Proceedings of the 1st Europe Conference, E-UNSAT 2008, Durham, United Kindom. London: Taylor and Francis, 2008, 291–288
8. Bardanis M E, Kavvadas M J. Modifying the Barcelona Basic Model to account for the residual void ratio and subsequent decrease of shear strength relative to suction. In: Toll D G, Augarde C E, Gallipoli D, Wheeler S J, eds. Proceedings of the 1st Europe Conference, E-UNSAT 2008, Durham, United Kindom. London: Taylor and Francis, 2008, 589–595
9. Zhou J. A study of applied pressure on the Soil Water Characteristic Curve. In: Toll D G, Augarde C E, Gallipoli D, Wheeler S J, eds. Proceedings of the 1st Europe Conference, E-UNSAT 2008, Durham, United Kindom. London: Taylor and Francis, 2008, 689–693
10. Delage P. Experimental unsaturated soils mechanics. In: Juca J F T, De Campos T M P, Marino F A M, eds. Proceedings of the 3rd International Conference on Unsaturated Soils, Recife, Brazil. Rotterdam: Balkema, 2002, 3: 973–998
11. Romero E, Vaunat J. Retention curves of deformable clays. In: Tarantino A, Macuso C, eds. Experimental Evidence and Theoretical Approaches in Unsaturated Soils, Trento, Italy. Rotterdam: Balkema, 2000, 91–106
12. Rampino C, Mancuso C, Vinale F. Laboratory testing on an unsaturated soil: equipment, procedures and first experimental results. Canadian Geotechnical Journal, 1999, 36(1): 1–12
13. Vanapalli S K, Fredlund D G, Pufahl D E. The influence of soil structure and stress history on the soil-water characteristics of a compacted till. Géotechnique, 1999, 49(2): 143–159
14. Ng C W W, Pang Y W. Experimental investigation of soil-water characteristics of a volcanic soil. Canadian Geotechnical Journal, 2000, 37(6): 1252–1264
15. Romero E. Characterization and thermo-hydro-mechanical behavior of unsaturated boom clay. Dissertation for the Doctoral Degree. Barcelona, Spain: Universitat Politècnica de Catalunya, 1999
16. Sun D A, Sheng D, Cui H B, Sloan S W. A density-dependent elastoplastic hydro-mechanical model for unsaturated compacted soils. International Journal for Numerical Analytical Method in Geomechanics, 2007, 31(11): 1257–1279
17. Huang S, Barbour S L, Fredlund D G. Development and verification of a coefficient of permeability function for a deformable unsaturated soil. Canadian Geotechnical Journal, 1998, 35(3): 411–425
18. Wheeler S J. Inclusion of specific water volume within an elasto-plastic model for unsaturated soil. Canadian Geotechnical Journal, 1996, 33(8): 42–57
19. Rampino C, Mancuso C, Vinale F. Experimental behavior and modeling of an unsaturated compacted soil. Canadian Geotechnical Journal, 2000, 37(4): 748–763
20. Barrera M. Estudio experimental del comportamiento hidromecánico de suelos colapsables. Dissertation for the Doctoral Degree. Barcelona, Spain: Universidad Politécnica de Catalunya, 2002
21. Sharma R S. Mechanical behavior of unsaturated highly expansive clays. Dissertation for the Doctoral Degree. Oxford, UK: University of Oxford, 1998
22. Sivakumar V. A critical state framework for unsaturated soil. Dissertation for the Doctoral Degree. Sheffield, UK: University of Sheffield, 1993
23. Kawai K, Kato S, Karube D. The model for water retention curve considering effects of void ratio. In: Rahardjo H, Toll D G, Leong E C, eds. Proceedings of the 1st Asian Conference on Unsaturated Soils, Singapore. Rotterdam: Balkema, 2000, 329–334
24. Gallipoli D, Gens A, Sharma R, Vaunat J. An elastoplastic model for unsaturated soil incoporating the effects of suction and degree of saturation on mechanical behavior. Géotechnique, 2003, 53(1): 123–135
25. Nitao J J, Bear J. Potentials and their role in transport in porous media. Water Resources Research , 1996, 32(2): 255–250
26. Buisson M S R, Wheller S J. Inclusion of hydraulic hysteresis in a new elasto-plastic framework for unsaturated soils. In: Tarantino A, Macuso C, eds. Experimental Evidence and Theoretical Approaches in Unsaturated Soils, Trento, Italy. Rotterdam: Balkema, 2000, 109–119
27. Topp G C. Soil water hysteresis in silt loam and clay loam soils. Water Resources, 1971, 7(4): 914–920
28. Gili J A, Alonso E E. Microstructural deformation mechanisms of unsaturated granular soils. International Journal for Numerical Analytical Method in Geomechanics, 2002, 26(5): 433–468
29. Skempton A W. Terzaghi's discovery of effective stress. In: Terzaghi K, ed. From Theory to Practice in Soil Mechanics. New York: John Wiley, 1960
30. Lade P V, De Boer R. The concept of effective stress for soil, concrete and rock. Géotechnique, 1997, 47(1): 61–78
31. Jennings J E B. Discussion on M.S. Youssef's paper, In: Proceedings of the 4th International Conference on Soil Mechanics, ISSMFE. 1957, 3: 168
32. Croney D, Coleman J D, Black W P M. Movement and distribution of water in soil in relation to highway design and performance. Highway Research Board, Spec. Report No. 40, 1958
33. Bishop A W. The principle of effective stress. Tecknisk Ukeblad, 1959, 106(39): 859–863
34. Aitchison G D. Relationships of moisture stress functions in unsaturated soils. In: Conference Pore Pressures, Institution of Civil Engineering. London: Buttherworths, 1960
35. Jennings J E B, Burland J B. Limitations to the use of effective stress in partly saturated soils. Géotechnique, 1962, 12(2): 125–144

36. Burland J B. Some aspects of the mechanical behavior of partly saturated soils. In: Aitchison G D, ed. Proceedings of the Conference on Moisture Equilibria and Moisture changes in the Soils Beneath Covered Areas, Australia. London: Butterworths, 1965, 270–278
37. Fredlund D G, Morgenstern N R. Stress state variables for unsaturated soils. Journal of Geotechnical Engineering Division, ASCE, 1977, 103 (GT5): 447–466
38. Alonso E E, Gens A, Josa A. A constitutive model for partially saturated soils. Géotechnique, 1990, 40(3): 405–430
39. Gens A, Alonso E E. A framework for the behavior of unsaturated expansive clays. Canadian Geotechnical Journal, 1992, 29: 1013–1032
40. Li X S. Thermodynamics-based constitutive framework for unsaturated soils. 2: A basic triaxial model. Géotechnique, 2007, 57(5): 423–435
41. Tamagnini R. An extended Cam-clay model for unsaturated soils with hydraulic hysteresis. Géotechnique, 2004, 54(3): 223–228
42. Öberg A-L, Sällfors G. A rational approach to the determination of the shear strength parameters of unsaturated soils. In: Alonso E, Delage P, eds. Proceedings of the 1st International Conference on Unsaturated Soils, Paris, France. Rotterdam: Balkema, 1995, 1: 151–158
43. Garven E A, Vanapalli S K. Evaluation of empirical procedures for predicting the shear strength of unsaturated soils. In: Proceedings of the 5th International Congress on Unsaturated Soil Mechanics. Arizona, USA: ASCE, 2006
44. Houlsby G. The work input to an unsaturated granular material. Géotechnique, 1997, 47(1): 193–196
45. Gray W G, Schrefler B A. Thermodynamics approach to effective stress in partially saturated porous media. European Journal of Mechanics-A/Solids, 2001, 20(4): 521–538
46. Laloui L, Klubertanz G, Vulliet L. Solid-liquid-air coupling in multiphase porous media. International Journal for Numerical and Analytical Methods in Geomechanics, 2003, 27(3): 183–206
47. Li X S. Effective stress in unsaturated soil: a microstructural analysis. Géotechnique, 2003, 53(2): 273–277
48. Coussy O. Poromechanics. Oxford, England: John Wiley & Sons, 2004
49. Alonso E E, Pereira J-M, Vaunat J, Olivella S. A microstructurally-based effective stress for unsaturated soils. Géotechnique (in press)
50. Rojas E. An equivalent stress equation for unsaturated soils. Part 1: The equivalent stress equation. International Journal of Geomechanics, ASCE, 2008, 8: 285–290
51. Haines W B. Studies in the physical properties of soils. II. A note on the cohesion developed by capillary forces in an ideal soil. The Journal of Agricultural Science, 1925, 15: 529–535
52. Murray E J. An equation of state for unsaturated soils. Canadian Geotechnical Journal, 2002, 39(1): 125–140
53. Desai C S, Wang Z. Disturbed state model for porous saturated materials. International Journal of Geomechanics, ASCE, 2003, 3(2): 260–265
54. Bishop A W, Alpan I, Blight G E, Donald I B. Factors controlling the strength of partly saturated cohesive soils. In: Conference on Stength of Cohesive Soils, Boulder, Colorado, USA. Arizona: ASCE, 1960, 503–532
55. Escario V, Saez J. The shear strength of partially saturated soils. Géotechnique, 1986, 36(3): 453–456
56. Gan J K M, Fredlund D G. Multistage direct shear testing of unsaturated soils. Geotechnical Testing Journal, 1988, 11(2): 132–138
57. Toll D G. A framework for unsaturated soil behavior. Géotechnique, 1990, 40(1): 31–44
58. Fredlund D G, Xing A, Fredlund M D, Barbour S L. The relationship of the unsaturated soil shear strength to the soil water characteristic curve. Canadian Geotechnical Journal, 1995, 33: 440–448
59. Miao L, Yin Z, Liu S. Empirical function representing the shear strength of unsaturated soils. Geotechnical Testing Journal, 2001, 24(2): 220–223
60. Toll D G, Ong B H. Critical-state parameters for an unsaturated residual sandy clay. Géotechnique, 2003, 53(1): 93–103
61. Tarantino A, Tombolato S. Coupling of hydraulic and mechanical behavior in unsaturated compacted clay. Géotechnique, 2005, 55 (4): 307–317
62. Vanapalli S K, Fredlund D G. Comparison of different procedures to predict the shear strength of unsaturated soils uses the soil-water characteristic curve. Geo-Denver 2000, American Society of Civil Engineers, Special Publication, 2000, 99: 195–209
63. Vaunat J, Romero E, Marchi C, Jommi C. In: Juca J F T, De Campos T M P, Marino F A M, eds. Proceedings of the 3rd International Conference on Unsaturated Soils, Recife, Brazil. Rotterdam: Balkema, 2002, 245–251
64. Tarantino A. A possible critical state framework for unsaturated compacted soils. Géotechnique, 2007, 57(4): 385–389
65. Han K K, Rahardjo H, Broms B B. Effect of hysteresis on the shear stength of a residual soil. In: Alonso E, Delage P, eds. Proceedings of the 1st International Conference on Unsaturated Soils, Paris, France. Rotterdam: Balkema, 1995, 499–504
66. Boso M. Shear strength behavior of a reconstituted partially saturated clayey silt. Dissertation for the Doctoral Degree. Trento, Italy: Università degli Studi di Trento, 2005
67. Romero E, Gens A, Lloret A. Water permeability, water retention curve and microstructure of unsaturated compacted Boom clay. Engineering Geology, 1999, 54(1–2):117–127
68. Sridharan A, Altschaeffl A G, Diamond S. Pore size distributions studies. Journal of the Soil Mechanics and Foundations Division, ASCE, 1971, 97(5): 771–787
69. Fisher R A. On the capillary forces in an ideal soil; correction of formulae given by W.B. Haines. The Journal of Agricultural Science, 1926, 16: 492–505
70. Karube D, Kato S. An ideal unsaturated soil and the Bishop's soil. In: Proceedings of the 13th International Conference on Soil. Mech. Found. Engng., New Delhi. 1994, 1:43–46
71. Karube D, Kawai K. The role of pore water in the mechanical behavior of unsaturated soils. Geotechnical and Geological Engineering, 2001, 19: 211–241
72. Chateau X, Dormieux L. Micromechanics of saturated and unsaturated porous media. International Journal for Numerical and Analytical Methods in Geomechanics, 2002, 26: 831–844
73. Molenkamp F, Nazemi A H. Interactions between two rough spheres, water bridge and water vapour. Géotechnique, 2003, 53

(2): 255–264
74. Wheeler S J, Sharma R S, Buisson M S R. Coupling hydraulic hysteresis and stress-strain behavior in unsaturated soils. Géotechnique, 2003, 53(1): 41–54
75. Alonso E E. Exploring the limits of unsaturated soil mechanics: The behavior of coarse granular soil and rockfill. The 11th Buchanan Lecture. University of Texas A&M, 2003
76. Oldecop L A, Alonso E E. A model for rockfill compressibility. Géotechnique, 2001, 51(2): 127–140
77. Oldecop L A, Alonso E E. Theoretical investigation of the time-dependent behavior of rockfill. Géotechnique, 2007, 57(3): 289–301
78. Chávez C, Alonso E E. A constitutive model for crushed granular aggregates which includes suction effects. Soils and Foundations, 2003, 43(4): 215–227
79. Suriol J, Gens A, Alonso E E. Behavior of compacted soils in suction-controlled oedometer. In: Technical Committee of the 2nd International Conference on Unsaturated Soils, eds. The Proceedings of the 2nd International Conference on Unsaturated Soils, Beijing, China. Netherlands: Springer, 1998, 438–443
80. Alonso E E, Vaunat J. An appraisal of structure level interactions in expansive soils. In: Ribeiro e Sousa L, Fernandes M M, Vargas E Jr., Azevedo R, eds. Applications of Computational Mechanics in Geotechncial Engineering, Proceedings of the 5th International Workshop, Guimaraes, Portugal. Rotterdam: Balkema, 2001,17–30
81. Alonso E E. Modeling expansive soil behavior. In: Technical Committee of the 2nd International Conference on Unsaturated Soils, eds. The Proceedings of the 2nd International Conference on Unsaturated Soils, Beijing, China. Netherlands: Springer, 1998, 37–70
82. Alonso E E, Vaunat J, Gens A. Modeling the mechanical behavior of expansive clays. Engineering Geology, 1999, 54: 173–183
83. Gens A. Constitutive modeling: application to compacted soils. In: Alonso E, Delage P, eds. Proceedings of the 1st International Conference on Unsaturated Soils, Paris, France. Rotterdam: Balkema, 1995, 1179–1200
84. Jommi C. Remarks on the constitutive modeling of unsaturated soils. In: Tarantino A, Macuso C, eds. Experimental Evidence and Theoretical Approaches in Unsaturated Soils, Trento, Italy. Rotterdam: Blakema, 2000, 139–154
85. Gens A, Sánchez M, Sheng D. On constitutive modeling of unsaturated soils. Acta Geotechnica, 2006, 1:137–147
86. Alonso E E, Gens A, Hight D W. General Report: The behavior of partially saturated soils. In: Hanrahan E T, Orr T L L, Widdis T F, eds. Proceedings of the 9th European Conference on Soil Mechanics and Foundations Engineering, Dublin. London: Taylor and Francis, 1987, 1087–1146
87. Alonso E E, Josa A Y, Gens A. Modeling the behavior of compacted soils upon wetting, Raul J. Marsal Volume, Soil Mech. Soc. of Mexico (SMMS), México. 1992
88. Sivakumar, V, Wheeler S J. Influence of compaction procedure on the mechanical behavior of an unsaturated compacted clay. Part 1: Wetting and isotropic compression. Géotechnique, 2000, 50(4): 359–368
89. Wheeler S, Sivakumar V. An elasto-plastic critical state framework for unsaturated soils. Géotechnique, 1995, 45(1): 35–53
90. Tarantino A, De Col E. Compaction behavior of clay. Géotechnique, 2008, 58(3): 199–213
91. Marsal R J, Arellano L R, Guzmán M A, Adame H. El Infernillo: Behavior of dams built in Mexico. Instituto de Ingeniería, UNAM, Mexico, 1976
92. Naylor D J, Maranha das Neves E, Mattar D, Veiga Pinto A A, Jr. Prediction of construction performance of Beliche Dam. Géotechnique, 1986, 36(3): 359–376
93. Naylor D J, Maranha das Neves E, Veiga Pinto A A. A back-analysis of Beliche Dam. Géotechnique, 1997, 47(2): 221–233
94. Soriano A, Sánchez F J. Settlements of railroad high embankments. In: Proceedings of XII European Conference on Soil Mechanics and Geotechnical Engineering, Netherlands. 1999
95. Justo J L, Durand P. Settlement-time behavior of granular embankments. International Journal for Numerical Analytical Method in Geomechanics, 2000, 24(3): 281–303
96. Leroueil S, Hight D W. Behavior and properties of natural soils and soft rocks. In: Hight D W, Leroueil S, Phoon K K, Tan T S, eds. Characterisation and Engineering Properties of Natural Soils, Proceedings of the International Workshop, Singapore. Swets and Zeitlinger, 2003, 29–254
97. Marsal R J. Large scale testing of rockfill materials. Journal of the Soil Mechanics and Foundation Division, ASCE, 1967, 93(2): 27–43
98. Charles J A, Watts K S. The influence of confining pressure on the shear strength of compacted rockfill. Géotechnique, 1980, 4(3): 353–398
99. De Mello V F B. Seventh Rankine Lecture: Reflections on design decisions of practical significance to embankment dams. Géotechnique, 1977, 27(3): 279–356
100. Hardin B O. Crushing of soil particles. Journal of Geotechnical Engineering, ASCE, 1985, 111(10): 1177–1192
101. Fumagalli E. Tests on cohesionless materials for rockfill dams. Journal of the Soil Mechanics and Foundations Division, ASCE , 1969, 95(SM1): 313–330
102. Marachi N D, Chan C K, Seed H B, Duncan J M. Strength and deformation characteristics of rockfill materials. Department of Civil Engineering, Report No. TE-69-5, University of California, 1969
103. Sowers G F, Williams R C, Wallace T S. Compressibility of broken rock and settlement of rockfills. In: Proceedings of the 6th ICSMFE, 2, Montreal. 1965, 561–565
104. Terzaghi K. Discussion on salt springs and lower bear riverdams. Transactions of ASCE, 1960, 125(2): 139–148
105. Veiga Pinto A A. Prediction of the structural behavior of rockfill dams. Dissertation of the Doctoral Degree. Lisbon, Portugal: National Laboratory of Civil Engineering, Portugal, 1983
106. Fredlund D G, Rahardjo H. Soil Mechanics for Unsaturated Soils. New York: John Wiley & Sons, 1993
107. Cundall P A, Strack O D L. A discrete numerical model for granular assemblies. Géotechnique, 1979, 29(1):47–65
108. Charles R J. Static fatigue of glass. Journal of Applied Physics, 1958, 29: 1549–1560
109. Mesri G, Godlewski P M. Time and stress compressibility interrelationship. Journal of the Geotechnical Engineering Division, 1977, 103(GT5): 417–430

110. McDowell G R. Micromechanics of creep of granular materials. Géotechnique, 2003, 53(10): 915–916
111. Chávez C. Estudio del comportamiento triaxial de materiales granulares de tamaño medio; con énfasis en la influencia de la succión. Dissertation for the Doctoral Degree. España: Universidad Politécnica de Cataluña, 2004
112. Cardoso R. Hydro-mechanical behavior of compacted marls. Dissertation for the Doctoral Degree. Lisbon: Instituto Superior Técnico, Lisbon Technical University, 2009
113. Cardoso R, Alonso E E. Degradation of compacted marls: a microstructural investigation. Soils and Foundations, 2009, 49(3): 315–327
114. Alonso E E, Alcoverro J. Swelling and degradation of argillaceous rocks. In: Juca J F T, De Campos T M P, Marino F A M, eds. Proceedings of the 3rd International Conference on Unsaturated Soils, Recif, Brazil. Rotterdam: Balkema, 2002, 37–70
115. Pinyol N M, Alonso E E, Vaunat J. A constitutive model for soft clayey rocks that includes weathering effects. Géotechnique, 2007, 57(2): 137–151
116. Burland J B. On the compressibility and shear strength of natural clays. Géotechnique, 1990, 40(3): 329–378
117. Alonso E E, Gens A. On the mechanical behavior of arid soils. In: Fookes P G, Parry R H, eds. Engineering Characteristics of Arid Soils, Proceedings of the 1st International Symposium, London. Rotterdam: Balkema, 1994, 173–206
118. van Genuchten M T. A closed-form equation for predicting the hydraulic conductivity of unsaturated soils. Soil Science Society of America Journal, 1980, 44(5): 892–898